Increasing heavy rainfall and extreme flood heights in a warming climate threaten densely populated regions across Sri Lanka and the Malacca Strait

Authors

Sarah Kew, *Royal Netherlands Meteorological Institute (KNMI), De Bilt, The Netherlands*
Mariam Zachariah, *Centre for Environmental Policy, Imperial College, London, UK*
Clair Barnes, *Centre for Environmental Policy, Imperial College, London, UK*
Lalith Rajapakse, *UNESCO Madanjeet Singh Centre for South Asia Water Management (UMCSAWM), University of Moratuwa, Sri Lanka*
Joseph Basconcillo, *Philippine Atmospheric, Geophysical and Astronomical Services Administration, Department of Science and Technology, Quezon City, Philippines*
Shiromani Jayawardena, *Regional Integrated Multi-Hazard Early Warning System for Africa and Asia (RIMES). Thailand*
Nurizana Amir Aziz, *Malaysian Meteorological Department (MET Malaysia), Petaling Jaya, Selangor, Malaysia*
Claire Bergin, *ICARUS Climate Research Centre, Maynooth University, Maynooth, Ireland*
Izidine Pinto, *Royal Netherlands Meteorological Institute (KNMI), De Bilt, The Netherlands*
Annalena Bacher, *Red Cross Red Crescent Climate Centre, The Hague, the Netherlands (based in Zug, Switzerland)*
Maja Vahlberg, *Red Cross Red Crescent Climate Centre, The Hague, the Netherlands; Swedish Red Cross, Stockholm, Sweden (based in Ubmeje/Umeå, Sweden)*
Aynur Kadihasanoglu, *Red Cross Red Crescent Climate Centre, The Hague, the Netherlands (based in Geneva, Switzerland)*
Ana Mejía, *Red Cross Red Crescent Climate Centre, The Hague, the Netherlands (based in Quito, Ecuador)*
Renate Meyer, *Red Cross Red Crescent Climate Centre, The Hague, the Netherlands (based in Cape Town, South Africa)*
Anka Stankovic, *Red Cross Red Crescent Climate Centre, The Hague, the Netherlands (based in Oxford, UK)*
Maléki Badjana, *Red Cross Red Crescent Climate Centre, The Hague, the Netherlands (based in Madagascar)*
Dora Vrkic, *Grantham Institute - Climate Change and the Environment, Imperial College, London, UK*
Emmanuel Raju, *Copenhagen Centre for Disaster Research, University of Copenhagen*

Jonatan Lassa, *Risk Science, Earth Sciences New Zealand (GNS Science), Aotearoa New Zealand*
Giriraj Amarnath, *International Water Management Institute (IWMI), Battaramulla, Sri Lanka*
Sjoukje Philip, *Royal Netherlands Meteorological Institute (KNMI), De Bilt, The Netherlands*

Review authors

Friederike Otto, *Centre for Environmental Policy, Imperial College, London, UK*
Ailsa Barrow-Kocher, *Met Office, Exeter, UK; Research and Evidence Directorate, Foreign, Commonwealth and Development Office (FCDO), London, UK*.
Dora Vrkic, *Grantham Institute - Climate Change and the Environment, Imperial College*
Roop Singh, *Red Cross Red Crescent Climate Centre, The Hague, The Netherlands (based in New Jersey, USA)*
David Rogers, *Independent Consultant, Switzerland*
Sajanika Sivanu, *Red Cross Red Crescent Climate Centre, The Hague, the Netherlands (based in Canada)*
Murugadas Loganathan*, British High Commission (based in Malaysia)*
Priyanka Dissanayake, *World Bank Sri Lanka/Netherlands Organization for Scientific Research (based in Colombo, Sri Lanka)*

Cite as Kew, S. et al., (2025): Increasing heavy rainfall and extreme flood heights in a warming climate threaten densely populated regions across Sri Lanka and the Malacca Strait (WWA scientific report No. 78) World Weather Attribution DOI: https://doi.org/10.25560/126259

Main findings

- Sri Lanka's flood risk stems from its steep central highlands and low-lying coastal plains. Intense rainfall quickly channelled runoff from the hills into densely populated floodplains. In the Malacca Strait region, the land is shaped by its vast archipelago of volcanic islands, broad plains, and deltas. With many islands having limited natural drainage, and deep valleys, heavy rainfall easily triggers both flash floods and landslides.
- In addition to climate change, extreme rainfall in this region is known to be influenced by ENSO and Indian Ocean Dipole (IOD). Therefore we first check whether these recurring climate variability patterns play a role. For the Strait of Malacca the occurrence of La Niña and a negative IOD this year, which both tend to enhance rainfall in this region, contributed to making the event more intense. We estimate that the current La Niña and negative IOD conditions contributed about 5% to 13% to observed rainfall.
- To estimate if human induced climate change influenced heavy rainfall over the Sri Lanka and the Malacca Strait regions we first determine if there is a trend in observations in the heaviest 5-day rainfall events. The extreme rainfall associated with Cyclonic Storm Senyar over Malacca Strait corresponds to roughly a 1-in-70-year event in today's climate. Over Sri Lanka, the extreme rainfall associated with Cyclonic Storm Ditwah corresponds to roughly a *1-in-30-year* event in today's climate. Local return periods can be much higher.
- To assess the role of climate change, we first examine whether there is a trend in the observations associated with the warming up until today of 1.3°C. Although different observations-based datasets show a wide range of trends, they all agree on the direction of change, suggesting that extreme rainfall spells are becoming more intense, in both study regions. For the Malacca Strait region, the increase in extreme rainfall associated with rising GMST is estimated at about 9% to 50%. Over Sri Lanka, the trends are even stronger; heavy 5 day precipitation events, such as those associated with Cyclonic Storm Ditwah, are now about 28% to 160% more intense due to the warming to date.
- To determine whether the observed trends can be attributed to human-driven climate change, we also assess high-resolution climate models that are known to capture rainfall patterns in the study regions best. However, models are not good at simulating the seasonal cycle over these small island regions, and the majority also do not capture the correlation with La Niña or the IOD. Over both study regions, these models do not show consistent results regarding the direction of change, so there are probably aspects of the atmospheric circulation that are systematically misrepresented by the models. This is surprising, given the substantial body of scientific literature reporting increases in heavy rainfall both within our study region and across the broader area.
- The large trend that is visible in the observations in both study regions is not captured in the models. This prevents us, without further detailed assessment of underlying processes and their representation in the climate models, to draw an overarching attribution conclusion that quantifies the influence of climate change on these events.
- Sea surface temperatures (SSTs) in the North Indian Ocean were observed to be about 0.2°C higher than 1991-2020 average, which will have added to the energy available for tropical storm development and evaporation leading to the heavy rainfall. Without the trend related to the 1.3°C rise in global temperatures, the SSTs would have been about one degree colder and below the 1991-2020 normal.

- Across both countries, rapid urbanization, large concentrations of people and assets in low-lying floodplains and deltas, and infrastructure built in or near frequently flooded corridors have elevated exposure to flood events.
- Cascading failures of transport, energy, communications, and basic services disproportionately affected low-income and marginalized groups, who are more likely to live in informal or substandard housing and to lack savings or insurance.
- While early warnings were issued in both Sri Lanka and Indonesia, failures in ICT infrastructure may have prevented them from reaching intended audiences, and even those who did receive warnings were often unable to anticipate the scale of the floods. Issues such as language barriers, timing of floods, and the remoteness of some communities presented further challenges.

1 Introduction

In November 2025, tropical cyclones (TCs) and seasonal monsoons brought extreme rainfall to large parts of Asia, triggering particularly severe flooding and landslides across Sri Lanka, large parts of Indonesia's Sumatra, northern peninsular Malaysia and southern Thailand towards the end of the month. More than 1600 lives were lost, hundreds remain missing, and the events left a trail of devastation across the region (The Economist, December 4, 2025).

In Sri Lanka, Cyclonic Storm Ditwah made landfall on 27 November, bringing strong winds and very heavy rainfall that caused the worst flooding and landslides since the early 2000s (ReliefWeb, 2025). As of December 8, at least 635 fatalities, 192 missing and over 233,000 displaced individuals are reported (DMC, Sri Lanka, 2025). Overall, at least 2,179,000 people have been affected across all 25 districts. The hardest hit districts are Gampaha, Colombo, Puttalam and Mannar, as well as Trincomalee and Batticaloa, while landslides in the central hill country have also affected Kandy, Badulla and Matale (UN News, 2025). Transport and energy infrastructure have been impaired across the country with at least 247 km of major roads and 35 bridges damaged and over 277,000 buildings inundated (ECHO, 2025; DMC Sri Lanka, 2025; News.lk, 2025). Sri Lanka's military as well as local and foreign aid organizations are supporting relief and rescue operations (BBC, 2025). Relief centres were set up and used by around 233,000 individuals (ReliefWeb, 2025). Access to clean water remains a major concern (UN News, 2025). The economic costs to rebuild infrastructure after the storm are estimated at six or seven billion USD (NYT, 2025a).

In Malaysia, Indonesia and Thailand, heavy rainfall, floods, and landslides have occurred over north-western Indonesia, Peninsular Malaysia and southern Thailand following an enhanced Northeast Monsoon and Cyclonic Storm Senyar, which made landfall in Indonesia on 26 November and Malaysia on 27 November (AHA Centre, 2025; The Straits Time, 2025). For Indonesia, at least 593 fatalities, 468 missing and 2,600 injured individuals as well as 600,000 displaced people have been reported by the International Federation of Red Cross and Red Crescent Societies (IFRC) as of December 2. Across the region, at least 5 million people are affected in total, with Sumatra being the hardest-hit region (ECHO, 2025; CNN, 2025). Senyar was preceded by high intensity monsoon rains, starting around November 23 (IFRC, 2025). The impacts of the storm were aggravated by soil instability and clogged drainage (IFRC, 2025). All affected provinces declared a state of emergency after November 26. Indonesia's police and military are conducting relief and rescue missions supported by various local and international organizations (IFRC, 2025).

From 22 November, Sri Lanka experienced torrential rainfall associated with the establishing Northeast Monsoon and intensified by Cyclonic Storm Ditwah (Figure 1.1). On the 26 of November, a well marked low pressure intensified into a depression over the southeastern coast of Sri Lanka, due to favourable conditions such as high sea surface temperatures over the region and mid-level vertical wind shear (IMD, 2025). Cyclonic Storm Ditwah made landfall on the island's east on 27 November 2025, bringing torrential rainfall and causing severe flooding in 25 districts and landslides (detailed information on the flooding extent and related impacts are kindly provided by the International Water Management Institute (IWMI) in appendix A1). Inundation levels were unprecedented, reaching 12-15 ft (about 3.5 - 4.5 m) in downstream parts of Malwathu Oya, Kala Oya, and Deduru Oya streams/rivers in the north central/western parts (Rajapakse, 2025, personal communication). In the north, western and central regions of the country, rainfall exceeded 350 mm in 24h (ReliefWeb, 2025, DMC, 2025).

From 22 to 28 November, Malaysia and Indonesia experienced persistent heavy rainfall, intensified by Cyclonic Storm Senyar (IMD, 2025), which developed near the Strait of Malacca, a tropical basin long considered almost cyclone-free, and moved slowly east (Figure 1.1). Its formation was aided by a strong north-east monsoon surge in the days preceding the storm, when bursts of cool continental air swept over the warm waters of the Malacca Strait, creating a shallow but coherent low-level circulation that allowed the rare equatorial cyclone to develop (AsiaNewsNetwork, December 3, 2025). While not extremely intense in wind strength, Senyar generated widespread torrential rainfall that led to severe flooding and landslides across Sumatra, Malaysia, and southern Thailand. As a result, Senyar caused far more extensive damage and loss of life, marking it as a more destructive but less equatorially extreme counterpart to Tropical Cyclone Vamei in 2001. TC Vamei formed at an exceptionally low latitude of about 1.4°N, making it one of the closest-to-equator TCs ever recorded (Zuki and Lupo, 2008).

Both systems formed unusually close to the equator, where the Coriolis force is typically insufficient to support organized cyclonic rotation. Their genesis was enabled by an exceptionally active Intertropical Convergence Zone (ITCZ), which provided persistent low-level convergence, deep convective clustering, and abundant moisture. Concurrently, equatorial waves (convectively coupled Kelvin waves) enhanced localized vorticity and vertical motion, effectively compensating for the weak background rotational forcing. Warm sea surface temperatures, high ocean heat content, and deep tropospheric moisture further supported rapid vortex organization and intensification.

After formation, both Ditwah and Senyar exhibited track behaviors typical of equatorial systems, including slow movement and irregular or looping trajectories resulting from weak steering currents near the equator. Cyclone Ditwah moved slowly northward across Sri Lanka along the eastern coastline, while Senyar oscillated south of Sumatra, allowing convective bands to persist over land and the Malacca Strait. These slow-moving tracks significantly amplified rainfall duration and flood potential, particularly when combined with orographic lifting in Sri Lanka's central highlands. Together, Ditwah and Senyar demonstrate that low-latitude cyclones now represent an emerging pathway for extreme rainfall and flood hazards in regions such as Sri Lanka and Indonesia.

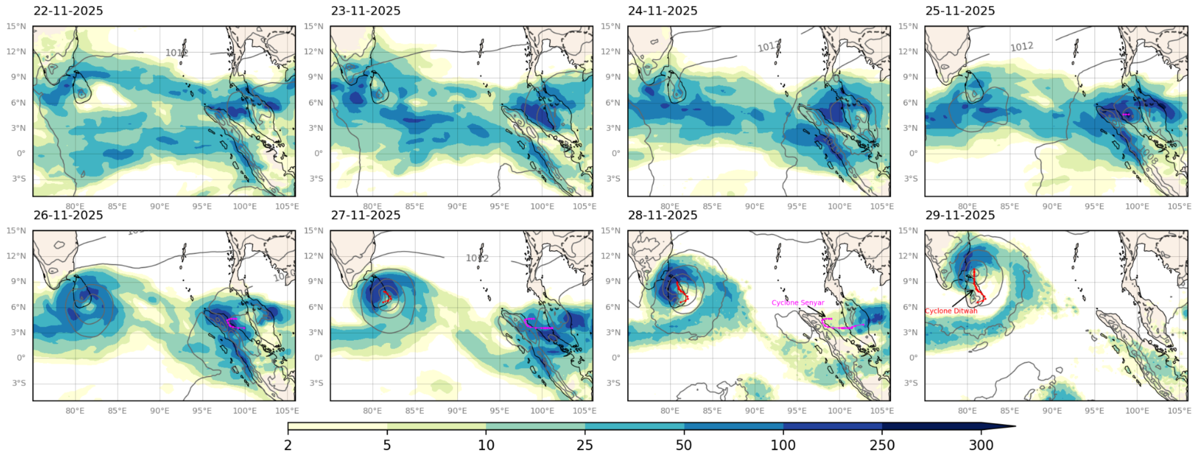

Figure 1.1. Daily rainfall and mean sea-level pressure from 22 to 29 November 2025. Cyclonic Storm Ditwah (red) is shown for 27-29 November, and Cyclonic Storm Senya (magenta) for 25-28 November. Data sources: ERA5 and IBTrACS

1.1 Rainfall extremes in Indonesia, Malaysia, Sri Lanka, and surrounding nations

Globally, there has been an increase in extreme precipitation events because of increased global temperatures. This observed increase follows the Clausius-Clapeyron principle, which states a 1°C rise in global temperatures equates to around a 7% increase in water retention by the atmosphere (Trenberth, 2011; Adam, 2023). Significant regional variability has been observed in Europe, Asia, Africa, and America (Alexander et al., 2006; Zhang et al., 2013; Donat et al., 2016). While regional variability exists, global trends indicate a rise in both the frequency and intensity of heavy precipitation, with projections showing further increases by the end of the century (Alexander et al., 2017; Seneviratne et al., 2021).This increase has also been observed over the South-East Asia region, where there has been an increase in the variability and extremity of rainfall over the period 1951 to 2014 (Singh and Xiaosheng, 2020).

Projections of extreme rainfall focussing on Indonesia (Kurniadi et al., 2023) showed large spatial and seasonal variations but overall suggest a continuous increase in wet extremes during the wet season, with upper extreme values surpassing records from the studied historical period of 1987-2014. In northern parts of Indonesia, where this study focuses, the wet season (December to February) is expected to become wetter and the dry season (June to August) drier. Breaking Indonesia into smaller regions, Marzuki et al., 2025 found rainfall increases in Central–Northern Sumatra are concentrated from November to February, coinciding with the peak monsoon season. These increases are also linked to enhanced moisture transport from the Indian Ocean and South China Sea.

Similar patterns were found in Malaysia, where Ng et al., 2022 found increasing trends in extreme precipitation and analysing 25 years of data, Tan, 2021 found an increasing trend in seasonal rainfall for Peninsular Malaysia. They also found spatial differences where interior dry regions are getting drier on average and coastal wet regions are getting wetter.

Across Sri Lanka, there is an overall increase in total annual rainfall with the strongest increase occurring in the eastern regions, as well as a marked upward trend during the First Inter-Monsoon (March to April) and North-East Monsoon seasons (December to February) (Abeysingha, 2022). Jayawardena et al. (2018) reported that extreme precipitation indicators, including maximum 1-day rainfall, maximum 5-day rainfall, and total precipitation on extreme rainfall days (R95p and R99p), exhibit increasing trends across most locations in Sri Lanka, indicating a rise in rainfall intensity.

There are two large-scale modes of climate variability that influence temperature, precipitation and winds in the study region - the Indian Ocean Dipole (IOD) and El Niño Southern Oscillation (ENSO). ENSO is a pattern of sea surface temperatures in the tropical Pacific Ocean that reoccurs every 2-7 years, tending to peak in December, with El Niño being the warm phase and La Niña the cooler phase. ENSO also influences the large-scale *atmospheric* movements in the tropical region - a cycle known as the Walker Circulation. During La Niña, the Walker Circulation intensifies leading to a strengthening of the upward motion of air (convection) over the Maritime Continent, which boosts storm formation in the region. La Niña also pushes warmer sea water towards the western Pacific Ocean, providing extra energy for tropical storms to form. The state of IOD and ENSO can interact, exacerbating their impacts. A negative IOD was officially declared by the Australian Bureau of Meteorology on 9 September 2025 (Bureau of Meteorology, 2025). A negative IOD is characterised by warmer waters in the east Indian Ocean with cooler waters in the west of the basin. The negative IOD was the strongest on record, since the Bureau's dataset began in 2008 (Bureau of Meteorology, 2025), likely contributing to the favorable conditions for storm development in the region.

1.2 Event Definition

In this study, we characterise the event in several ways in order to capture the rainfall associated with the cyclones that caused the majority of the reported impacts, and also the sea surface temperature conditions feeding moisture into the cyclones.

Rainfall:
To best understand the effect of heavy rainfall across parts of south-east Asia and Sri-Lanka we split the spatial domain into two main regions. Yearly maximum 5-day precipitations are used for both regions, based on the observed event. The event definitions are as follows:

- The Malacca Strait: A polygonal domain was defined encompassing the northern part of the island of Sumatra in Indonesia and most of the Malaysian peninsula and the southernmost parts of Thailand (hereafter, the Malacca Strait region), to capture the regions that experienced the worst impacts due to the heavy rain fall during Storm Senyar. The annual (Jul-Jun) maximum 5-day rainfall total (Rx5day) was chosen to reflect the duration of the rainfall from Storm Senyar in this region.
- Sri Lanka: the entire island of Sri Lanka is used as the second study area. A yearly (Jul-Jun) maximum 5-day accumulation period was chosen to capture the impacts of the rainfall in Sri Lanka associated with Storm Ditwah.

Both study regions can be seen in Fig. 1.2. These two regions cover some of the the major impact sites including Trincomalee, Batticaloa, Mannar, and Jaffna in Sri Lanka; and Kelantan, Terengganu, Pahang, North Sumatra, West Sumatra, Songkhla, Pattani, and Narathiwat in Malaysia, Sumatra, and Thailand.

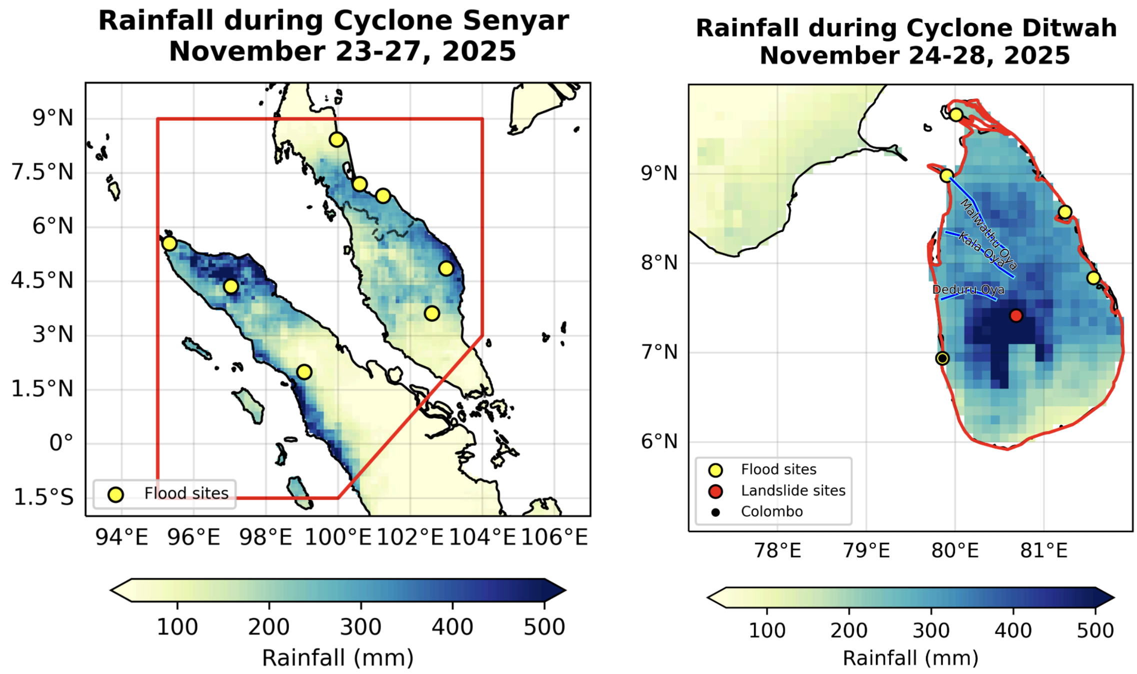

Figure 1.2*: Event definition maps of 5-day precipitation associated with Cyclonic Storms Senyar and Ditwah, in the Malacca Strait region and Sri Lanka, respectively. Blue lines show the approximate locations along which flooding occurred. Left: Box over Sumatra, Indonesia, Malaysia and southern Thailand with south-east triangle cut out. Right: Island of Sri Lanka. Data source: MSWEP*

Sea surface temperatures

Warm Sea Surface Temperatures (SSTs) increase evaporation, adding more moisture to the atmosphere. This extra moisture often leads to heavier and more frequent rainfall in nearby regions. At the time of the events, the region is under the influence of the negative phase of the IOD and La Niña, both of which are associated with positive SST anomalies in the region. Therefore we additionally investigate SSTs in the Northern Indian Ocean in observations. The event definition is as follows:

- Northern Indian Ocean: November mean SSTs averaged over the region covering the Northern Indian ocean between and encompassing Sri Lanka and the Malacca Strait, defined by a box (see Fig. 6.1a) extending from 77°E to 105°E and from 0°N to 15°N.

2. Data and methods extreme rainfall

2.1 Data

In this report, we study the influence of anthropogenic climate change by comparing the likelihood and intensity of similar rainfall extremes at present with those in a 1.3°C cooler climate. We also extend this analysis into the future by assessing the influence of a further 1.3°C of global warming.

2.1.1 Observational data

We first use observational and reanalysis data to estimate the return period of a similar event in the present day and to assess the historical trends with increasing Global Mean Surface Temperature (GMST). The datasets used are as follows:

1. **ERA5:** The European Centre for Medium-Range Weather Forecasts's 5th generation reanalysis product, ERA5, is a gridded dataset that combines historical observations into global estimates using advanced modelling and data assimilation systems (Hersbach et al., 2020). We use precipitation data from this product at a resolution of 0.5°×0.5°, from the years 1950 to present.
2. **CPC:** We use CPC daily precipitation. This is the gridded product from NOAA PSL, Boulder, Colorado, USA known as the CPC Global Unified Daily Gridded data, available at 0.5° x 0.5° resolution, for the period 1979-present. Data are available from NOAA.
3. **MSWEP:** The Multi-Source Weighted-Ensemble Precipitation (MSWEP) v2.8 dataset (updated from Beck et al., 2019) is fully global, available at 3-hourly intervals and at 0.1° spatial resolution, available from 1979 to ~3 hours from real-time. This product combines gauge-, satellite-, and reanalysis-based data, including ERA5.
4. **CHIRPS:** The rainfall product developed by the UC Santa Barbara Climate Hazards Group called "Climate Hazards Group InfraRed Precipitation with Station data" (CHIRPS; Funk et al. 2015). Daily data are available at 0.05° resolution, from 1981-31 October 2025. The product incorporates satellite imagery with in-situ station data.

As a measure of anthropogenic climate change we use the (low-pass filtered) global mean surface temperature (GMST), where GMST is taken from the National Aeronautics and Space Administration (NASA) Goddard Institute for Space Science (GISS) surface temperature analysis (GISTEMP, Hansen et al., 2010 and Lenssen et al. 2019).

As a measure of the El Niño - Southern Oscillation cycle (ENSO) we use the detrended Niño3.4 index. This is computed from NOAA's ERSST v.5 sea surface temperatures, by subtracting the mean tropical SST (20S-20N) from the mean SST over the Niño3.4 region (5S-5N, 170W-120W). This index is therefore adjusted to remove the linear trend associated with climate change as proposed in van Oldenborgh et al., 2021, but without rescaling each calendar month.

Time series of the observed Indian Ocean Dipole (IOD) derived from the ERSST dataset were obtained from KNMI's Climate Explorer tool.

2.1.2 Model and experiment descriptions

We use two multi-model ensembles from climate modelling experiments using very different framings (Philip et al., 2020): Sea Surface temperature (SST) driven global circulation high resolution models and regional climate models.

HighResMIP SST-forced model ensemble (Haarsma et al. 2016), the simulations for which span from 1950 to 2050. The SST and sea ice forcings for the period 1950-2014 are obtained from the 0.25° x 0.25° Hadley Centre Global Sea Ice and Sea Surface Temperature dataset that have undergone area-weighted regridding to match the climate model resolution. For the 'future' time period (2015-2050), SST/sea-ice data are derived from RCP8.5 (CMIP5) data, and combined with greenhouse gas forcings from SSP5-8.5 (CMIP6) simulations (see Section 3.3 of Haarsma et al. 2016 for further details).

Coordinated Regional Climate Downscaling Experiment CORDEX-CORE over the West-Asia domain with 0.22 km resolution (WAS-22) (Teichman et al., 2021) and with 0.44 km resolution (WAS-44). The ensemble used consists of WAS-22 and WAS-44 together with different combinations of 5 regional climate models and downscaling 11 GCMS, resulting in 26 combinations. These simulations are composed of historical simulations up to 2005, and extended to the year 2100 using the RCP8.5 scenario.

2.2 Statistical methods

Methods for observational and model analysis and for model evaluation and synthesis are used according to the World Weather Attribution Protocol, described in Philip et al., (2020), with supporting details found in van Oldenborgh et al., (2021), Ciavarella et al., (2021) and Otto et al., (2024). The key steps, presented in sections 3-6, are: (3) trend estimation from observations; (4) model validation; (5) multi-method multi-model attribution; and (6) synthesis of the attribution statement.

In this report we analyse time series of Rx5day over the Malacca Strait region and over Sri Lanka.

For both regions a nonstationary Generalised Extreme Value (GEV) distribution is used to model Rx5day. The precipitation distribution is assumed to scale exponentially with the covariates, with the dispersion (the ratio between the standard deviation and the mean) remaining constant over time (e.g., Philip et al., 2018; Luu et al., 2021). The parameters of the statistical model are estimated using maximum likelihood.

For each time series we calculate the return period and intensity of the event under study for the 2025 GMST and for 1.3°C cooler GMST: this allows us to compare the climate of now and of the preindustrial past (1850-1900, based on the Global Warming Index), by calculating the probability ratio (PR; the factor-change in the event's probability) and change in intensity of the event.

In order to examine the effect of the ENSO and IOD phase on Rx5day alongside that of increasing GMST, we extend the nonstationary model to accommodate additional covariates. The variable of interest, X, is assumed to follow a GEV distribution in which the location and scale parameters vary with both GMST, ENSO and IOD:

$$X \sim GEV(\mu, \sigma, \xi \mid \mu_0, \sigma_0, \alpha, \beta, \gamma, T, N, I),$$

where X denotes the variable of interest, rainy-season precipitation; T is the smoothed GMST; N is the detrended Niño3.4 index; I is the IOD index; μ_0, σ_0 and ξ are the location, scale and shape parameters of the nonstationary distribution; and α, β and γ are the trends due to GMST, ENSO, and IOD respectively. As a result, the location and scale of the distribution have a different value in each year, determined by the GMST, Niño3.4 and IOD states each year. Maximum likelihood estimation is used to estimate the model parameters, with

$$\mu = \mu_0 exp\left(\frac{\alpha T + \beta N + \gamma I}{\mu_o}\right) \quad \text{and} \quad \sigma = \sigma_0 exp\left(\frac{\alpha T + \beta N + \gamma I}{\mu_o}\right).$$

This formulation reflects the Clausius Clapeyron relation, which implies that precipitation scales exponentially with temperature (Trenberth et.al., 2003, O'Gorman and Schneider 2009), and so that precipitation will scale exponentially with the all three of the explanatory covariates. In this study, we design the model so as to consider the contribution from GMST vs the joint contributions resulting from ENSO and IOD. This means for contributions from GMST, we hold the ENSO and IOD indices we set both β and γ to zero while to get the contribution from ENSO+IOD we set α to zero.

Under this model, the effects of GMST are independent of the effects of the detrended Niño3.4 index and the IOD index, so that the change in intensity due to GMST is unaffected by the change in intensity due to the ENSO or IOD phase. We note that this may not be the case in the real world, as the intensity and frequency of El Niño events may have been influenced by climate change (Cai et al., 2021); however, by using a detrended Niño3.4 index (see Section 2.1) we aim to minimise the correlation between the two factors, and so do not expect the qualitative findings of this study to be affected by this simplifying assumption. ENSO and the IOD are known to be positively correlated, and so the effects of these two factors cannot be separated by this model; however, the cumulative effect of ENSO and IOD together can still be estimated.

We also analyse November-mean SSTs of Northern Indian Ocean in the region extending from 77°E to 105°E and from 0°N to 15°N, using the Gaussian distribution to statistically model the SST trends. The SST distribution is assumed to shift linearly with the covariates, while the variance remains constant.

3. Analysis extreme rainfall

3.1 Observational analysis: return period and trend

Four gridded datasets, MSWEP, ERA5, CPC and CHIRPS, were used in this analysis, all with the exception of CHIRPS containing both events, at the time of doing this analysis. All four datasets are found to be in overall agreement in the trends and year-to-year variability (figure 3.1). However, their absolute magnitudes differ. For example, ERA5 (blue markers) consistently underestimates the highest rainfall peaks in both regions compared to the other datasets, while CHIRPS tends to show larger peaks in rainfall in Sri Lanka, compared to the other datasets. Given the small size of the study domains, their tropical setting with frequent storms, and the complex topography, it is unsurprising that gridded products differ. Satellite-based datasets can be affected by cloud cover, while the quality of gauge-based datasets depend on the number, distribution, and quality of ground stations. Additionally, interpolation and merging techniques may limit their ability to fully capture local rainfall extremes. However, using these datasets together is expected to average out some of their individual biases and provide a more robust estimate of the rainfall characteristics.

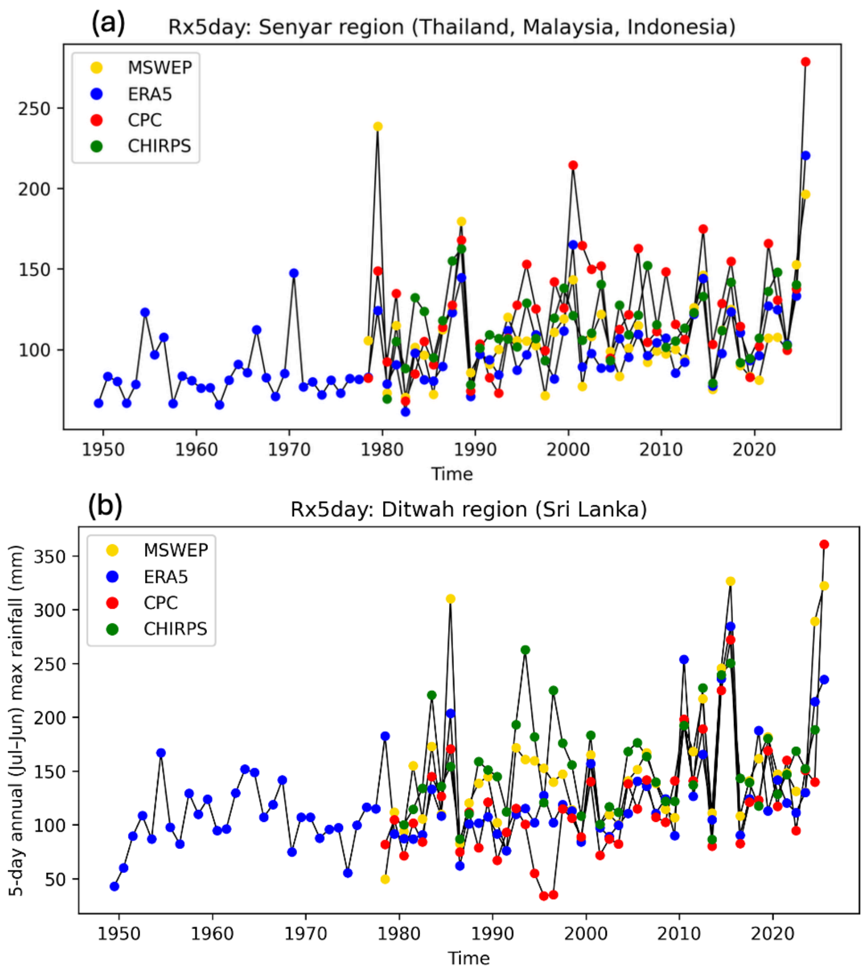

Figure 3.1: *Rx5day annual time series for the Malacca Strait (a) and Sri Lanka(b) regions for MSWEP, ERA5, CPC and CHIRPS.*

The IOD and ENSO are important drivers of rainfall amounts associated with the monsoon, as well as the number of storms developing in this region during the season. During Cyclones Senyar and Ditwah, the simultaneous presence of La Niña and a negative IOD appears to have played a significant role in fueling the storms and amplifying the associated rainfall extremes. Therefore, for this analysis, in addition to GMST, we also test the effects of ENSO and IOD on extreme rainfall events in the study regions.

3.1.1 Analysis of gridded data: Malacca Strait region

We first tested three non-stationary models using different covariates: GMST-only, GMST+ENSO, and GMST+IOD. However, due to the positive correlation between ENSO and IOD (r ~ 0.56) and their well-known influence on rainfall in these regions, it is difficult to disentangle their individual contributions, with different datasets showing greater sensitivity to one or the other. Therefore, we designed a fourth non-stationary model that includes GMST, ENSO, and IOD as covariates, allowing us to decompose the contributions from GMST and the combined effects of ENSO and IOD phases (as discussed in Section 2.2).

Figure 3.2 (a,d,g,j) shows the evolution of annual (Jul-Jun) Rx5day events in the study region in time for the four datasets, overlaid with model estimated values. The statistical model is able to track the year-to-year variability in the observations in all datasets, emphasising the importance of ENSO+IOD in driving rainfall extremes in this domain. The middle and the right panels show annual Rx5day rainfall vs GMST and the return level plots in today's climate and a 1.3°C cooler climate that is representative of the pre-industrial climate, assuming that the ENSO and IOD conditions remain stationary at the observed 2025 conditions. All datasets suggest that rainfall extremes in the region have increased with 1.3°C warming, albeit with large uncertainties, and at different rates in the different datasets (bigger changes in ERA5 (Fig. 3.2 (f)) and CPC (Fig. 3.2 (i)) as compared to MSWEP (Fig. 3.2 (c)) and CHIRPS (Fig. 3.2 (l)).

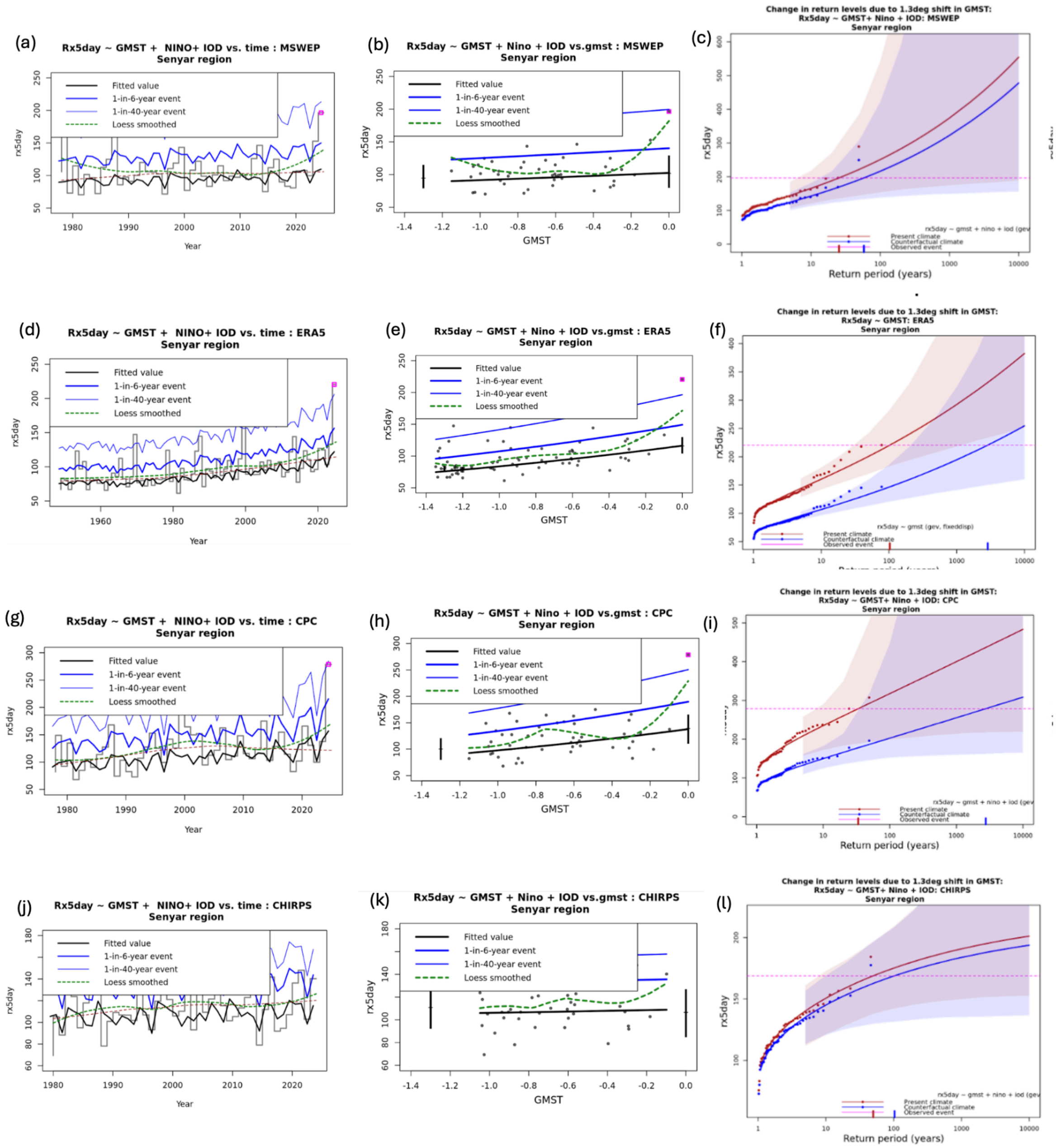

***Figure 3.2**: GEV fit with fixed dispersion parameter scaling proportional to GMST, Niño3.4 and IOD of the index series. Figures a, d, g and j show the evolution of annual (Jul-Jun) Rx5day over the Malacca Strait overlaid with model estimates. Figures b, e, h and k show Rx5day as a function of the smoothed GMST. The thick black line denotes the time-varying location parameter. The vertical black*

lines show the 95% confidence interval for the location parameter, for the current, 2025 climate and the fictional, 1.3ºC cooler climate. The 2025 observation is highlighted with the magenta box. Figures c, f, i and l show the return time plots for the climate of 2025 (red) and a climate with GMST 1.3ºC cooler (blue). The past observations are shown twice: once shifted up to the current climate and once shifted down to the climate of the pre-industrial era. The markers show the data and the lines show the fits and uncertainty from the bootstrap. The magenta line shows the magnitude of the 2025 event analysed here. These are shown for (from top to bottom) MSWEP, ERA5, CPC and CHIRPS.

Table 3.1 shows the summary of the findings from the four observed datasets. In today's climate characterised by current warming levels and the observed La Niña and negative IOD conditions, the Rx5day event has return periods ranging from 25 to 65 years across the different datasets. Based on this range we estimate that the return period of the Rx5day event under the 2025 conditions is about 50 years. Due to the absence of good quality and sufficiently long station records that we were unable to access on the rapid time scales of this analysis, we cannot validate the exact rate of increase. However, it should be noted that despite the wide uncertainty range in the individual datasets and the wide range in the best estimates of return periods for the 2025 event in the four datasets, all of these show positive trends, suggesting that there is indeed an increasing tendency of extreme rainfall due to global warming. We infer that the 2025 event has been made about 2 to 80 times more likely and 4 to 60% more intense due to human-induced climate change, assuming the IOD and ENSO conditions remain unchanged. Relative to neutral ENSO and IOD states, the prevailing negative IOD and La Niña conditions also appear to have increased the likelihood and intensity of the event, by 1.5 to 5 times in PR and by 5 to 13% in intensity.

Dataset	Event		GMST		ENSO+IOD combined effect	
	Magnitude (mm/5day)	Return period (years)	Probability Ratio	Change in magnitude (%)	Probability Ratio	Change in magnitude (%)
MSWEP	196.476	25 (7 to 41910)	2.3 (0.11 to inf)	16 (-22.7 to 67.17)	**1.5 (1.1 to 66.5)**	**7.7 (2 to 13.8)**
ERA5	220.516	65 (22 to 637)	**25.5 (5.1 to 13149)**	**53.3 (33.9 to 79)**	1.5 (0.9 to 2.9)	5.3 (-1.5 to 10.2)
CPC	278.703	33 (8 to inf)	**82.2 (2.2 to inf)**	**56.7 (11 to 107.5)**	**2.7 (1.2 to inf)**	**12.6 (3.3 to 20.4)**
CHIRPS	168.88	50	2.1 (0 to inf)	3.8 (-24.3 to 38.6)	**5.1 (1.2 to inf)**	**8 (1.8 to 14.1)**

Table 3.1: Change in probability ratio and magnitude for the Malacca Strait region due to both GMST and ENSO and IOD combined. Significant changes are indicated in bold. The 95% confidence intervals are given in brackets.

Figure 3.3 and Table 3.2 summarize the trend-fitting results for Rx5day in the Malacca Strait, using a simplified non-stationary GEV model with only GMST as the covariate. Even with this simplified model, all four datasets consistently show an increase in extreme rainfall associated with global warming. The return period of the 2025 event in today's climate ranges from 33 to 103 years. Based on this range we estimate the return period of the Rx5day event in today's climate, taking GMST only into account, to be about 70 years. Based on the trend-fitting results, we conclude that the 2025 event has been made approximately 2 to 30 times more likely and 9 to 50% more intense due to human-induced climate change. These estimates are nearly identical to those from the GMST+ENSO+IOD model, suggesting that although more of the variability is explained by adding in the ENSO and IOD covariates, this does not significantly influence the trend due to GMST. Consequently, this simplified model is sufficient to describe the relationship between rainfall extremes and climate change in the region. For the model analysis we adopt the rounded return period of 70 years as the event definition for the attribution analysis with climate models.

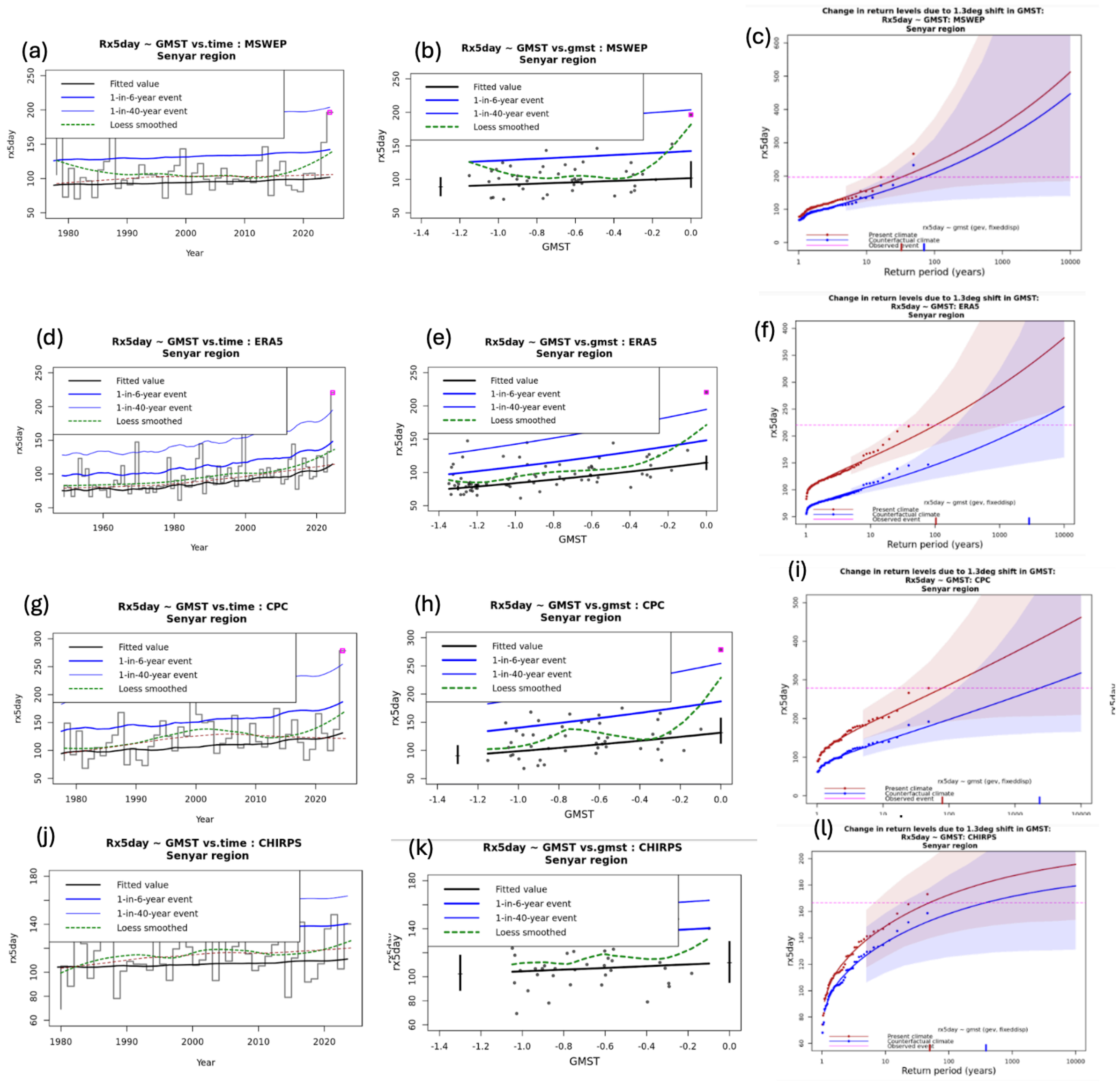

Figure 3.3: *GEV fit with fixed dispersion parameter scaling proportional to GMST of the index series. Figures a, d, g and j show the evolution of annual (Jul-Jun) Rx5day over the Malacca Strait overlaid*

with model estimates. Figures b, e, h and k show Rx5day as a function of the smoothed GMST. The thick black line denotes the time-varying location parameter. The vertical black lines show the 95% confidence interval for the location parameter, for the current, 2025 climate and the fictional, 1.3ºC cooler climate. The 2025 observation is highlighted with the magenta box. Figures c, f, i and l show the return time plots for the climate of 2025 (red) and a climate with GMST 1.3ºC cooler (blue). The past observations are shown twice: once shifted up to the current climate and once shifted down to the climate of the pre-industrial era. The markers show the data and the lines show the fits and uncertainty from the bootstrap. The magenta line shows the magnitude of the 2025 event analysed here. These are shown for (from top to bottom) MSWEP, ERA5, CPC and CHIRPS.

Dataset	Event		GMST	
	Magnitude (mm/5day)	Return period (years)	Probability Ratio	Change in magnitude (%)
MSWEP	196.476	33 (10 to inf)	2.2 (0.2 to inf)	14.6 (-19 to 66.7)
ERA5	220.516	103 (31 to 1216)	**27.9 (4.5 to 64368)**	**50.2 (32 to 73)**
CPC	278.703	79 (17 to inf)	**29.7 (1.6 to inf)**	**45.3 (5.3 to 108.3)**
CHIRPS	166.73	70	7.7 (0 to inf)	9.1 (-15.5 to 49.2)

Table 3.2: Change in probability ratio and magnitude for the Malacca Strait region for the statistical model with only GMST. Significant changes are indicated in bold. The 95% confidence intervals are given in brackets.

3.1.2 Analysis of gridded data: Sri Lanka

We follow the same analytical approach used for the Malacca Strait event (Section 3.1.1) to assess whether, and to what extent, rainfall extremes in Sri Lanka are influenced by increasing GMST. When evaluating the performance of different non-stationary statistical models in representing the distribution and trends of annual (July–June) area-averaged Rx5day over Sri Lanka, we find that the GMST-only model is sufficient to capture the long-term trends. In this case, adding IOD and ENSO as additional covariates does not meaningfully improve the model's ability to explain the observed rainfall variability or trends. Therefore we use this model for the subsequent analysis.

Fig. 3.4 and Table 3.3 summarize the trend-fitting results for Rx5day in Sri Lanka, based on a non-stationary GEV model with only GMST as the covariate. All datasets suggest that rainfall extremes in the region have increased in this region due to 1.3°C warming, albeit with large uncertainties, and at different rates in the different datasets (bigger changes in MSWEP (Fig. 3.4 (c)) and CPC (Fig. 3.4 (i)) as compared to ERA5 (Fig. 3.4 (f)) and CHIRPS (Fig. 3.4 (l)). Consequently, the return period of the 2025 event in today's climate also varies between the datasets ranging from 3 years in ERA5 to 43 years in CPC. We use a rounded estimate of 30 years to define this event for attribution analysis using climate models.

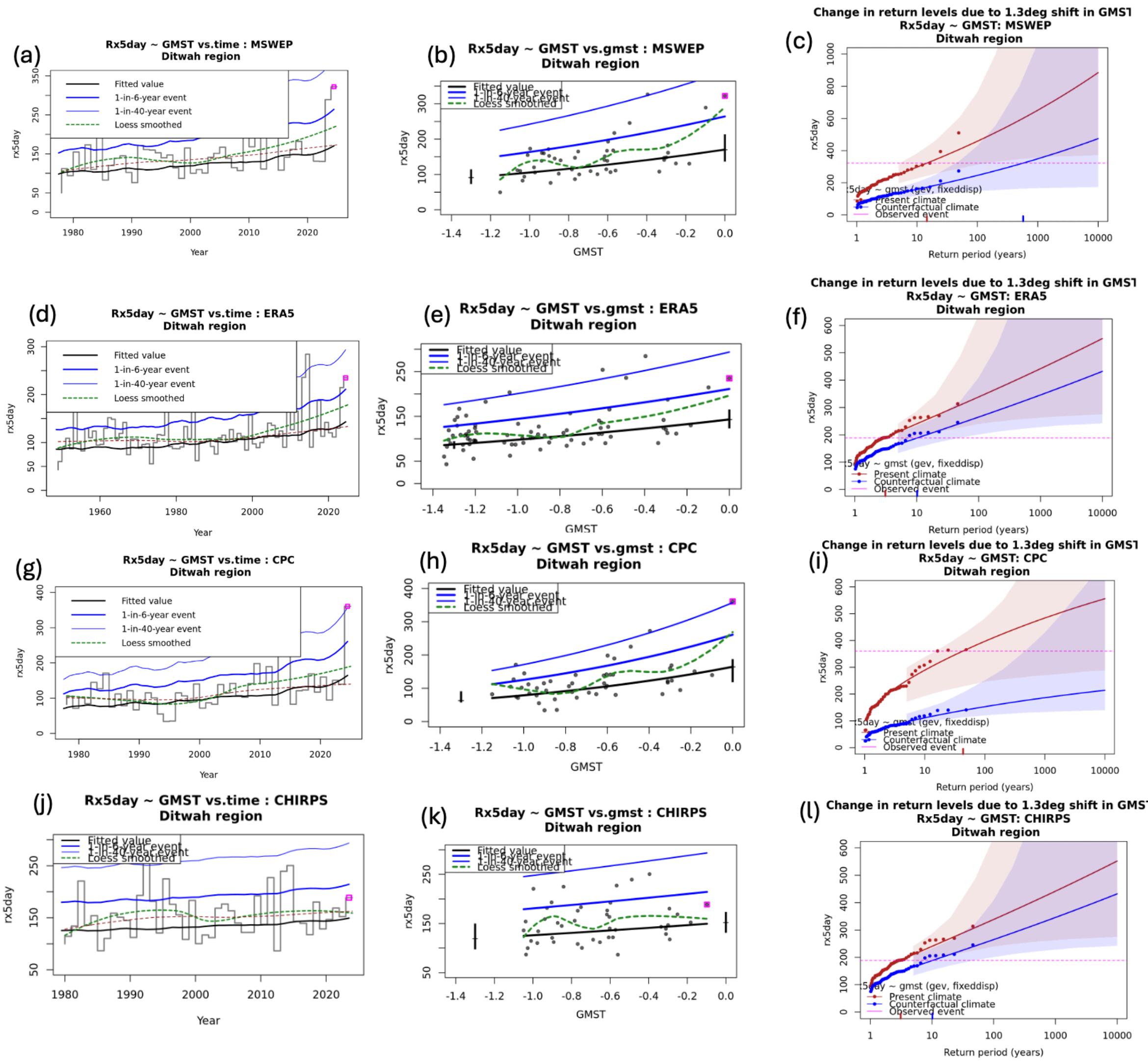

Figure 3.4: *GEV fit with fixed dispersion parameter scaling proportional to GMST of the index series. Figures a, d, g and j show the evolution of annual (Jul-Jun) Rx5day over Sri Lanka overlaid with model estimates. Figures b, e, h and k show Rx5day as a function of the smoothed GMST. The thick black line denotes the time-varying location parameter. The vertical black lines show the 95% confidence interval for the location parameter, for the current, 2025 climate and the fictional, 1.3ºC cooler climate. The 2025 observation is highlighted with the magenta box. Figures c, f, i and l show the return time plots for the climate of 2025 (red) and a climate with GMST 1.3ºC cooler (blue). The past observations are shown twice: once shifted up to the current climate and once shifted down to the climate of the pre-industrial era. The markers show the data and the lines show the fits and uncertainty from the bootstrap. The magenta line shows the magnitude of the 2025 event analysed here. These are shown for (from top to bottom) MSWEP, ERA5, CPC and CHIRPS.*

The best estimated PR and intensity change along with the 5-95% confidence intervals between today's climate and a hypothetical 1.3ºC cooler climate representative of the pre-industrial climate suggest an increase in likelihood and intensity of maximum extreme 5-day rainfall in Sri Lanka associated with increasing GMST. The increases are highest in the MSWEP and CPC datasets, with a best estimated 39-fold increase in the likelihood and and 86.5% increase in rainfall amount in today's climate as compared to the pre-industrial climate in MSWEP and an infinite increase in likelihood (lower bound of 9) and 160% increase in the intensity in CPC. In the ERA5 dataset, events such as the one under study are now 3 times more likely and about 30% more intense. Assuming a return period of 30 years as the event definition, CHIRPS also track a similar 30% increase in the 30-year event in today's climate as compared to the pre-industrial climate.

Dataset	Event		GMST	
	Magnitude (mm/5day)	Return period (years)	Probability Ratio	Change in magnitude (%)
MSWEP	322.26	15 (5 to 147)	39.2 (3.1 to inf)	86.5 (27.8 to 196.4)
ERA5	188.57	3 (2 to 9)	3.3 (0.5 to 18.6)	27.8 (-13.1 to 75.1)
CPC	221.79	43 (15 to inf)	Inf (9 to inf)	159.7 (48.6 to 249.6)
CHIRPS	286.85	30	6(0.3 to inf)	27.78 (-10.95 to 75.08)

Table 3.3: Change in probability ratio and magnitude for Sri Lanka for the statistical model with only GMST. Significant changes are indicated in bold. The 95% confidence intervals are given in brackets.

From analysing trends in the observations, we detect increasing trends in extreme rainfall associated with GMST, for both regions and in all four datasets considered in the study. In the next sections we use climate models to carry out attribution analysis to confirm whether and to what extent these trends can be attributed to human-induced climate change

4 Model evaluation

In the subsections below we show the results of the model evaluation for each location. For each framing or model setup we also use models that only just pass the evaluation tests if we only have five models or less for that framing that perform well. As per our protocol, all available climate models are evaluated against the observations in their ability to capture rainfall characteristics prior to inclusion for the attribution analysis based on: 1. Seasonal cycles (we discard models that exhibit ill-defined peaks and the ones that have a different rainy season onset/termination). 2. Spatial patterns (we discard models that are not able to capture the climatological precipitation patterns). 3 Parameters of the fitted statistical models (we discard the model if the model and observation parameters ranges do not overlap). 4. Correlation with modes of variability: As an additional criterion, we also filter the models based on whether they are able to capture the correlations between rainfall and ENSO and rainfall and IOD, which exist in the observations, when studying events in regions where there are known influences. The models are labelled as ‘good’,‘reasonable’, or ‘bad’ based on their performances in terms of the criteria discussed above. A model is given an overall rating of ‘good’ if it is rated ‘good’ for the first three characteristics (or for all four when correlation is assessed as well). If there is at least one ‘reasonable’, then its overall rating will be ‘reasonable’ and ‘bad’ if there is at least one ‘bad’. Per framing or model setup we also use models that only just pass the validation tests if we only have five models or less for that framing that perform well.

In this study, however, none of the available models were able to satisfactorily reproduce the observed seasonal cycle. In addition, the large uncertainties in the statistical parameters likely stemming from differences in record length, magnitude, and strength of trends across observational datasets, make it difficult to meaningfully distinguish models based on their ability to simulate rainfall distributions. Around half of the CORDEX models also failed to reproduce the observed correlations with ENSO and IOD. Therefore, instead of a full evaluation, we adopt a more lenient filtering approach, discarding only those models that clearly misrepresent the timing of the early or late rainfall peaks, fail to capture the bimodal structure, or substantially misrepresent the dry summer months.

Following this approach, using the statistical model with only GMST as a covariate and a return period of 70 years for Malacca Strait and 30 years for Sri Lanka, the tables show the model evaluation results for the two study regions, and ranking the remaining ones as good if they follow the observed cycle closely, and reasonable if they follow the shape broadly.

4.1 Malacca Strait region

Model / Observations	Seasonal cycle	Dispersion	Shape parameter	Conclusion
CHIRPS		0.185 (0.132 ... 0.220)	-0.21 (-0.50 ... -0.0072)	
ERA5		0.159 (0.118 ... 0.185)	0.095 (-0.038 ... 0.30)	
MSWEP		0.205 (0.159 ... 0.235)	0.15 (-0.25 ... 0.38)	
HighResMIP ()		(...)	(...)	
highresSST_CMCC-CM2-HR4_r1i1p1f1_gn ()		0.210 (0.179 ... 0.247)	0.044 (-0.15 ... 0.22)	good
highresSST_CNRM-CM6-1_r1i1p1f2_gr ()		0.138 (0.110 ... 0.160)	0.066 (-0.10 ... 0.20)	good
highresSST_CNRM-CM6-1-HR_r1i1p1f2_gr ()		0.163 (0.123 ... 0.189)	-0.017 (-0.16 ... 0.19)	good
highresSST_HadGEM3-GC31-HM_r1i2p1f1_gn ()		0.129 (0.105 ... 0.147)	-0.040 (-0.25 ... 0.12)	good
highresSST_HadGEM3-GC31-HM_r1i3p1f1_gn ()		0.115 (0.0932 ... 0.135)	0.017 (-0.26 ... 0.19)	reasonable
CORDEX ()		(...)	(...)	

SEA-22_CNRM-CM5_r1i1p1_RCA4 ()	good	0.128 (0.103 ... 0.154)	0.39 (0.16 ... 0.62)	reasonable
SEA-22_EC-EARTH_r1i1p1_RegCM4-3 ()	reasonable	0.155 (0.111 ... 0.180)	-0.038 (-0.21 ... 0.23)	reasonable
SEA-22_GFDL-ESM2M_r1i1p1_RegCM4-3 ()	reasonable	0.154 (0.0997 ... 0.184)	0.21 (0.0057 ... 0.65)	reasonable
SEA-22_HadGEM2-ES_r1i1p1_RCA4 ()	good	0.183 (0.149 ... 0.214)	-0.058 (-0.26 ... 0.12)	good
SEA-22_HadGEM2-ES_r1i1p1_RegCM4-3 ()	bad	0.126 (0.104 ... 0.144)	-0.077 (-0.33 ... 0.056)	bad
SEA-22_HadGEM2-ES_r1i1p1_RegCM4-7 ()	reasonable	0.0901 (0.0697 ... 0.105)	0.051 (-0.38 ... 0.25)	bad
SEA-22_HadGEM2-ES_r1i1p1_REMO2015 ()	good	0.186 (0.141 ... 0.216)	0.049 (-0.16 ... 0.29)	good
SEA-22_IPSL-CM5A-LR_r1i1p1_RegCM4-3 ()	bad	0.119 (0.0987 ... 0.135)	0.056 (-0.23 ... 0.24)	bad
SEA-22_MPI-ESM-LR_r1i1p1_REMO2015 ()	bad	0.218 (0.158 ... 0.258)	-0.11 (-0.30 ... 0.21)	bad
SEA-22_MPI-ESM-MR_r1i1p1_RegCM4-3 ()	reasonable	0.107 (0.0818 ... 0.127)	0.10 (-0.14 ... 0.32)	reasonable
SEA-22_MPI-ESM-MR_r1i1p1_RegCM4-7 ()	bad	0.159 (0.0978 ... 0.190)	-0.11 (-0.29 ... 0.33)	bad
SEA-22_NorESM1-M_r1i1p1_RegCM4-7 ()	reasonable	0.236 (0.182 ... 0.274)	-0.061 (-0.29 ... 0.22)	reasonable
SEA-22_NorESM1-M_r1i1p1_REMO2015 ()	reasonable	0.260 (0.189 ... 0.302)	-0.052 (-0.36 ... 0.43)	reasonable

Table 4.1: Evaluation results of the climate models considered for attribution analysis of Jun-Jul Rx5day for the Malacca Strait. For each model, the threshold for a 1-in-70-year event is shown, along with the best estimates of the Dispersion and Shape parameters are shown, along with 95% confidence intervals. Furthermore evaluation of the seasonal cycle and spatial pattern are shown.

4.2 Sri Lanka

Model / Observations	**Seasonal cycle**	**Dispersion**	**Shape parameter**	**Conclusion**

CHIRPS		0.249 (0.170 ... 0.299)	0.029 (-0.25 ... 0.45)	
ERA5		0.249 (0.170 ... 0.299)	0.029 (-0.25 ... 0.45)	
MSWEP		0.300 (0.212 ... 0.362)	0.085 (-0.28 ... 0.44)	
HighResMIP ()		(...)	(...)	
highresSST_CMCC-CM2-HR4_r1i1p1f1_gn ()		0.356 (0.298 ... 0.406)	0.16 (-0.011 ... 0.32)	
highresSST_CNRM-CM6-1_r1i1p1f2_gr ()		0.321 (0.266 ... 0.369)	0.0059 (-0.16 ... 0.16)	
highresSST_CNRM-CM6-1-HR_r1i1p1f2_gr ()		0.253 (0.208 ... 0.291)	-0.050 (-0.21 ... 0.11)	
highresSST_HadGEM3-GC31-HM_r1i2p1f1_gn ()		0.222 (0.173 ... 0.254)	0.070 (-0.10 ... 0.26)	
highresSST_HadGEM3-GC31-HM_r1i3p1f1_gn ()		0.253 (0.199 ... 0.299)	0.052 (-0.12 ... 0.24)	
CORDEX ()		(...)	(...)	
WAS-22_EC-EARTH_r12i1p1_COSMO ()	bad	0.253 (0.202 ... 0.288)	0.096 (-0.070 ... 0.26)	bad
WAS-22_HadGEM2-ES_r1i1p1_REMO2015 ()	bad	0.192 (0.151 ... 0.224)	-0.081 (-0.35 ... 0.12)	bad
WAS-22_MIROC5_r1i1p1_RegCM4-7 ()	bad	0.197 (0.156 ... 0.237)	0.29 (0.057 ... 0.57)	bad
WAS-22_MPI-ESM-LR_r1i1p1_COSMO ()	reasonable	0.397 (0.280 ... 0.464)	0.26 (0.11 ... 0.75)	reasonable
WAS-22_MPI-ESM-LR_r1i1p1_REMO2015 ()	bad	0.378 (0.285 ... 0.452)	0.13 (-0.53 ... 0.40)	bad
WAS-22_MPI-ESM-MR_r1i1p1_RegCM4-7 ()	reasonable	0.239 (0.158 ... 0.293)	0.52 (0.33 ... 1.0)	reasonable
cordex ()	bad	0.374 (0.312 ... 0.418)	0.18 (-0.015 ... 0.38)	bad
WAS-22_NorESM1-M_r1i1p1_RegCM4-7 ()	bad	0.190 (0.120 ... 0.227)	0.10 (-0.31 ... 0.39)	bad
WAS-22_NorESM1-M_r1i1p1_REMO2015 ()	bad	0.336 (0.196 ... 0.415)	-0.087 (-0.33 ... 0.32)	bad
WAS-44_CanESM2_r1i1p1_RCA4 ()	good	0.362 (0.274 ... 0.424)	0.34 (0.12 ... 0.66)	good
WAS-44_CanESM2_r1i1p1_RegCM4-4 ()	bad	0.279 (0.228 ... 0.318)	0.11 (-0.11 ... 0.32)	bad

WAS-44_CNRM-CM5_r1i1p1_RCA4 ()	reasonable	0.219 (0.158 ... 0.264)	0.46 (0.29 ... 0.80)	reasonable
WAS-44_CNRM-CM5_r1i1p1_RegCM4-4 ()	bad	0.244 (0.189 ... 0.285)	0.34 (0.16 ... 0.61)	bad
WAS-44_CSIRO-Mk3-6-0_r1i1p1_RCA4 ()	reasonable	0.509 (0.429 ... 0.578)	0.39 (0.17 ... 0.62)	reasonable
WAS-44_CSIRO-Mk3-6-0_r1i1p1_RegCM4-4 ()	bad	0.264 (0.202 ... 0.304)	0.087 (-0.10 ... 0.32)	bad
WAS-44_EC-EARTH_r12i1p1_RCA4 ()	reasonable	0.355 (0.288 ... 0.412)	0.41 (0.14 ... 0.67)	reasonable
WAS-44_GFDL-ESM2M_r1i1p1_RCA4 ()	reasonable	0.326 (0.262 ... 0.376)	0.45 (0.19 ... 0.76)	reasonable
WAS-44_GFDL-ESM2M_r1i1p1_RegCM4-4 ()	bad	0.270 (0.215 ... 0.313)	0.17 (0.013 ... 0.32)	bad
WAS-44_HadGEM2-ES_r1i1p1_RCA4 ()	reasonable	0.298 (0.246 ... 0.342)	0.19 (-0.10 ... 0.44)	reasonable
WAS-44_IPSL-CM5A-LR_r1i1p1_RegCM4-4 ()	bad	0.318 (0.255 ... 0.368)	0.15 (-0.026 ... 0.35)	bad
WAS-44_IPSL-CM5A-MR_r1i1p1_RCA4 ()	reasonable	0.355 (0.264 ... 0.406)	0.25 (0.071 ... 0.57)	reasonable
WAS-44_MIROC5_r1i1p1_RCA4 ()	reasonable	0.351 (0.275 ... 0.417)	0.49 (0.29 ... 0.76)	reasonable
WAS-44_MPI-ESM-LR_r1i1p1_RCA4 ()	reasonable	0.324 (0.242 ... 0.397)	0.74 (0.56 ... 1.1)	bad
WAS-44_MPI-ESM-LR_r1i1p1_REMO2009 ()	bad	0.274 (0.211 ... 0.313)	0.11 (-0.042 ... 0.37)	bad
WAS-44_MPI-ESM-MR_r1i1p1_RegCM4-4 ()	bad	0.293 (0.235 ... 0.341)	0.40 (0.20 ... 0.61)	bad
WAS-44_NorESM1-M_r1i1p1_RCA4 ()	reasonable	0.313 (0.242 ... 0.368)	0.29 (0.023 ... 0.54)	reasonable

Table 4.2.: Evaluation results of the climate models considered for attribution analysis of Jun-Jul Rx5day for Sri Lanka. For each model, the threshold for a 1-in-30-year event is shown, along with the best estimates of the Dispersion and Shape parameters are shown, along with 95% confidence intervals. Furthermore evaluation of the seasonal cycle and spatial pattern are shown.

5 Multi-method multi-model attribution

This section shows Probability Ratios and change in intensity ΔI for models that passed model evaluation and also includes the values calculated from the fits with observations.

5.1 Malacca Strait region

Model / Observations	Past vs.present		Present vs. future	
	Probability ratio PR [-]	Change in intensity ΔI [%]	Probability ratio PR [-]	Change in intensity ΔI [%]
CHIRPS	7.7 (0.0 ... ∞)	9.1 (-16 ... 49)		
ERA5	28 (4.5 ... 6.4e+4)	50 (32 ... 73)		
MSWEP	2.2 (0.21 ... ∞)	15 (-19 ... 67)		
highresSST_CMCC-CM2-HR4_r1i1p1f1_gn ()	0.91 (0.89 ... 4.4)	-1.2 (-1.5 ... 16)	0.90 (0.87 ... 2.6)	-1.2 (-1.8 ... 11)
highresSST_CNRM-CM6-1_r1i1p1f2_gr ()	0.75 (0.49 ... 2.1)	-3.1 (-7.0 ... 8.6)	0.76 (0.51 ... 1.2)	-3.2 (-7.4 ... 2.1)
highresSST_CNRM-CM6-1-HR_r1i1p1f2_gr ()	0.69 (0.43 ... 2.0)	-3.4 (-6.8 ... 6.3)	0.50 (0.26 ... 0.95)	-5.6 (-9.3 ... -0.40)
highresSST_HadGEM3-GC31-HM_r1i2p1f1_gn ()	3.6 (0.69 ... 2.2e+2)	9.2 (-3.1 ... 20)	3.3 (1.9 ... 6.8)	9.2 (4.7 ... 14)
highresSST_HadGEM3-GC31-HM_r1i3p1f1_gn ()	8.1 (2.1 ... ∞)	18 (6.2 ... 29)	5.1 (2.5 ... 19)	13 (8.3 ... 17)
SEA-22_CNRM-CM5_r1i1p1_RCA4 ()	1.1 (0.78 ... 1.6)	2.4 (-5.9 ... 12)	0.99 (1.4 ... 7.1)	3.5 (-0.31 ... 7.2)
SEA-22_EC-EARTH_r1i1p1_RegCM4-3 ()	0.34 (0.070 ... 2.1)	-9.1 (-25 ... 5.8)	0.51 (1.5 ... -5.9)	-2.1 (-7.8 ... 3.9)
SEA-22_GFDL-ESM2M_r1i1p1_RegCM4-3 ()	1.3 (0.53 ... 3.2)	5.4 (-10 ... 22)	0.54 (1.1 ... -8.9)	-3.4 (-9.8 ... 1.8)
SEA-22_HadGEM2-ES_r1i1p1_RCA4 ()	2.3 (0.45 ... 15)	7.1 (-5.3 ... 21)	1.0 (4.3 ... 13)	4.6 (0.26 ... 10)
SEA-22_HadGEM2-ES_r1i1p1_REMO2015 ()	0.53 (0.20 ... 2.7)	-7.6 (-21 ... 11)	0.45 (1.0 ... -13)	-5.1 (-11 ... 0.24)
SEA-22_MPI-ESM-MR_r1i1p1_RegCM4-3 ()	0.19 (0.033 ... 0.58)	-17 (-24 ... -7.2)	0.28 (0.93 ... -11)	-4.9 (-8.7 ... -0.66)
SEA-22_NorESM1-M_r1i1p1_RegCM4-7 ()	2.4 (0.14 ... 6.4e+2)	8.4 (-18 ... 48)	0.86 (4.5 ... 19)	7.7 (-2.2 ... 16)

SEA-22_NorESM1-M_r1i1p1_REMO2015 ()	0.91 (0.044 ... 16)	-1.0 (-30 ... 46)	0.26 (2.1 ... 4.4)	1.3 (-8.7 ... 11)

Table 5.1.: Probability ratio and change in intensity for 70-year return period for Jun-Jul Rx5day for the Malacca Strait, for observational datasets and each model that passed the evaluation tests. (a) from pre-industrial climate to the present and (b) from the present to 2.6℃ above pre-industrial climate.

5.2 Sri Lanka

Model / Observations	Past vs.present		Present vs. future	
	Probability ratio PR [-]	**Change in intensity ΔI [mm/5day]**	**Probability ratio PR [-]**	**Change in intensity ΔI [%]**
CHIRPS	6.3 (0.040 ... ∞)	28 (-11 ... 75)		
ERA5	3.3 (0.46 ... 19)	28 (-13 ... 75)		
MSWEP	39 (3.1 ... ∞)	86 (28 ... 2.0e+2)		
WAS-22_MPI-ESM-LR_r1i1p1_COSMO ()	2.0 (0.90 ... 5.3)	25 (-5.5 ... 55)	1.1 (2.2 ... 56)	12 (2.3 ... 20)
WAS-22_MPI-ESM-MR_r1i1p1_RegCM4-7 ()	1.7 (0.99 ... 2.5)	26 (-0.49 ... 47)	0.99 (1.3 ... 51)	7.9 (-0.53 ... 15)
WAS-44_CanESM2_r1i1p1_RCA4 ()	0.91 (0.48 ... 1.8)	-3.4 (-20 ... 19)	0.79 (1.2 ... -4.3)	-1.0 (-7.8 ... 5.8)
WAS-44_CNRM-CM5_r1i1p1_RCA4 ()	1.3 (0.81 ... 1.9)	10 (-8.0 ... 27)	1.0 (1.6 ... 19)	6.6 (1.1 ... 14)
WAS-44_CSIRO-Mk3-6-0_r1i1p1_RCA4 ()	1.3 (0.37 ... 5.4)	12 (-36 ... 88)	1.7 (3.8 ... 1.7e+2)	28 (18 ... 37)
WAS-44_EC-EARTH_r12i1p1_RCA4 ()	2.0 (1.0 ... 4.3)	33 (0.025 ... 72)	1.1 (1.5 ... 59)	11 (4.1 ... 17)
WAS-44_GFDL-ESM2M_r1i1p1_RCA4 ()	1.5 (0.79 ... 3.2)	19 (-8.8 ... 53)	1.1 (1.6 ... 70)	13 (3.8 ... 19)
WAS-44_HadGEM2-ES_r1i1p1_RCA4 ()	2.0 (0.88 ... 9.5)	17 (-2.7 ... 42)	1.3 (1.8 ... 50)	13 (7.7 ... 17)
WAS-44_IPSL-CM5A-MR_r1i1p1_RCA4 ()	2.1 (0.89 ... 5.8)	24 (-3.8 ... 60)	1.1 (1.9 ... 36)	9.3 (2.6 ... 16)
WAS-44_MIROC5_r1i1p1_RCA4 ()	1.6 (0.86 ... 4.0)	26 (-7.5 ... 70)	1.2 (1.6 ... 65)	13 (6.5 ... 18)
WAS-44_MPI-ESM-LR_r1i1p1_RCA4 ()	1.2 (0.97 ... 1.4)	15 (-2.3 ... 31)	1.1 (1.4 ... 87)	13 (7.4 ... 17)

WAS-44_NorESM1-M_r1i1p1_RCA4 ()	2.2 (0.59 ... 5.8)	28 (-11 ... 68)	1.1 (2.7 ... 41)	11 (1.8 ... 20)

Table 5.2.: Probability ratio and change in intensity for 30-year return period for Jun-Jul Rx5day for Sri Lanka, for observational datasets and each model that passed the evaluation tests. (a) from pre-industrial climate to the present and (b) from the present to 2.6℃ above pre-industrial climate.

6 Analysis of SST in the Northern Indian Ocean

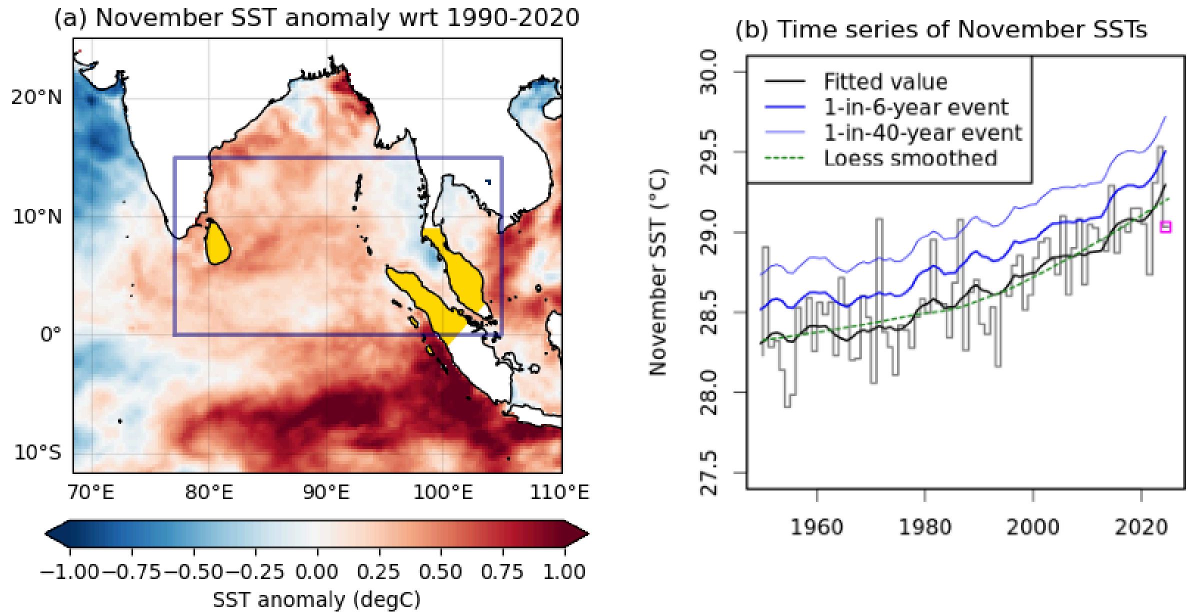

Figure 6.1: (a) Map of November 2025 SST anomalies with respect to the 1990-2020 climatology (ERA5). The two land regions in the study are highlighted in yellow. (b) Time series of November mean SSTs averaged over the box outlined in blue, with (Normal) fitted model overlaid. The pink dot marks November 2025; the heavy black line indicates the expected SST, given the GMST in that year, and the blue lines indicate the expected return levels of 1-in-6- and 1-in-40- year events. The green line is a nonparametric Loess smoother. All data from ERA5.

Figure 6.1a shows the SST anomalies in the Northern Indian Ocean during November 2025, with respect to the 1991-2020 climatology; the region within the box outlined in blue, where Cyclonic Storms Senyar and Ditwah formed, was around 29°C, which is on average 0.2°C higher than the 1991-2020 average. Figure 6.1b shows the average November SSTs over the box, overlaid with outputs from a fitted model in which the SSTs are assumed to be Normally distributed and to depend linearly on GMST. The fitted trend line (in black) follows the nonparametric trend over time (in green), indicating that the observed increase in November SSTs closely follows what is predicted based on increasing global temperatures. Figure 6.1b shows that in November 2025 (pink dot), the SSTs were actually somewhat cooler than is now expected for the time of year (see green Loes smoothed curve), although global warming means that expected temperatures for the time of year are now around 0.5°C warmer than between 1991-2020 (and around 1°C warmer than they would have been in a 1.3°C cooler climate without human-caused warming).

To test whether ENSO or the IOD might also be affecting SSTs in this region, we repeated the model fitting process using ENSO and IOD as additional covariates (see Section 2.2 for details of the model formulation, although here it was used with a Normal distribution that shifts linearly with GMST, ENSO and IOD). The results of this model fitting are shown in Table 6.1. GMST alone accounts for around 60% of the total variability in the time series, with IOD and ENSO accounting for a further

10% between them. Adding ENSO and IOD to the model makes very little difference to the estimated contribution from global warming, with the region now on average 1°C warmer than it would have been in a 1.3°C cooler climate (95% confidence interval: 0.76°C, 1.1°C). SSTs in this region are generally expected to be warmer than the average when ENSO and the IOD are negative, as they were in September-November 2025. In the box under study, the correlation between SST and ENSO and IOD is low, and the statistical model indicates a small insignificant signal wrt Nino3.4, IOD and the combined effect. Nonetheless, SSTs as warm as these would have been extremely unlikely without human-caused warming, with even the most conservative model finding that similarly warm temperatures are now at least 140 times more likely to occur than they would have been in a 1.3°C cooler climate.

	Probability ratio		**Change in intensity**		
	2025 vs PI	**2025 vs neutral**	**2025 vs PI**	**2025 vs neutral**	**% variance explained**
GMST only	1200 (140, 70000)	-	0.95 (0.76, 1.1)	-	60 (44, 74)
GMST + Nino3.4	10000 (4200, 6.1e+07)	0.91 (0.78, 0.98)	1 (0.85, 1.2)	-0.12 (-0.18, -0.07)	71 (59, 81)
GMST + IOD	21000 (960, 5700000)	0.84 (0.66, 0.97)	0.9 (0.73, 1.1)	-0.092 (-0.15, -0.039)	67 (52, 79)
GMST + Nino3.4 + IOD	190000 (4700, 4.3e+08)	0.86 (0.68, 0.97)	0.98 (0.83, 1.1)	-0.14 (-0.2, -0.074)	71 (58, 82)

Table 6.1: *Probability ratio and change in intensity in SSTs comparing the 2025 climate with a 1.3°C cooler climate without human-caused warming, and with a neutral ENSO and IOD state; proportion of the variance in the time series explained by each combination of factors.*

7 Hazard summary

For the two rainfall event definitions over the Malacca Strait and Sri Lanka described above, we evaluate the influence of anthropogenic climate change on the events as observed in 2025 by calculating the probability ratio as well as the change in intensity using observations and climate models. Models which do not pass the evaluation described above are excluded from the analysis. The aim is to synthesise results from models that pass the evaluation along with the observations-based products, to give an overarching attribution statement.

Figures 7.1 and 7.2 show the changes in intensity for the observations (blue) and models (red). Before combining them into a synthesised assessment, first, a representation error is added (in quadrature) to the observations, to account for the difference between observations-based datasets that cannot be explained by natural variability. This is shown in these figures as white boxes around the light blue bars. The dark blue bar shows the average over the observation-based products. Next, a term to account for intermodel spread is added (in quadrature) to the natural variability of the models. This is shown in the figures as white boxes around the light red bars. The dark red bar shows the model average, consisting of a weighted mean using the (uncorrelated) uncertainties due to natural variability plus the term representing intermodel spread (i.e., the inverse square of the white bars).

Observation-based products and models are combined into a single result in two ways. Firstly, we neglect common model uncertainties beyond the intermodel spread that is depicted by the model average, and compute the weighted average of models (dark red bar) and observations (dark blue bar): this is indicated by the magenta bar. As, due to common model uncertainties, model uncertainty can be larger than the intermodel spread, secondly, we also show the more conservative estimate of an unweighted, direct average of observations (dark blue bar) and models (dark red bar) contributing 50% each, indicated by the white box around the magenta bar in the synthesis figures.

For the synthesis we only use results from the statistical model that only includes GMST as a covariate.

Although the spread between the trend in the four observational datasets is large, all four observational datasets clearly show trends towards more rainfall in Rx5day. For the Malacca Strait, as shown in Section 3.1.1, the best estimates of the intensity change associated with global warming range from 4% to 60% when using the full statistical model that includes GMST together with ENSO and IOD as covariates. The simplified GMST-only model produces very similar results, with estimates ranging from 9% to 50%, indicating that although including ENSO and IOD explains more of the year-to-year variability, it does not discernibly affect the long-term trend driven by GMST. In addition, the climate models struggle to simulate the seasonal cycle and the rainfall–ENSO/IOD correlations reliably. For these reasons, we adopt the simpler GMST-only model for the models, as it captures the warming-related trend without the added uncertainty of poorly represented modes of variability. For Sri Lanka, the nature of change is again qualitatively similar to the Malacca Strait region (based on GMST-only model, which is also the best-performing model for the region; see Section 3.1.2). The four datasets all indicate trends towards more precipitation, with best estimates ranging from 28%-160%. Results for probability ratio are less confined (not shown), therefore we focus on intensity changes only.

Due to the spread in the intensity changes in observations the uncertainty around the synthesised intensity changes for observations only are quite large, however, the best estimates are very high compared to other studies on attributing Rx5day events, see Table 7.1. The synthesised observations indicate trends of almost 30% (-15% to 100%) for Malacca Strait and almost 70% (-25% to 250%) for Sri Lanka which is between 3 and 7 times more than the 10% increase due to 1.3°C of warming until now expected from the Clausius-Clayperon relationship.

Models show different behaviour than the observation-based datasets. For the Malacca Strait, all models indicate no trend, and for Sri Lanka, the HighResMIP models indicate no trend. Meanwhile, the Cordex models show small insignificant trends, with slightly larger uncertainties than the HighResMIP models. Synthesised model results are therefore close to no trend. However, we know models are not capturing the seasonal cycle of rainfall well, and the physical processes driving tropical heavy rainfall are not fully captured in the models. Also, models are usually less able to represent rainfall over islands than over larger continental regions. This is similar to what we found in a previous rainfall study for the Philippines (Zachariah. et al., 2024). As expected, analysis of the model future does not change this picture. Because models do not capture the observed trends we cannot combine these into a synthesised statement.

For SSTs over the Northern Indian Ocean the picture from observations is also clear. According to the observations-only analysis this region now has SSTs that are 1°C warmer than in a 1.3°C cooler climate. This trend likely contributed to the trend in the observed rainfall.

The large trends in rainfall in observations is expected to include the contribution from the Clausius-Clayperon relation that prescribes that a warmer atmosphere can hold more moisture and thus lead to more precipitation. Since the climate models do not mirror this trend, we do not provide a synthesised statement of the role of anthropogenic climate change, as we cannot quantify the role of climate change with the available models. Nonetheless, we conclude that climate change is at least one driver of the observed trend given that the other major known drivers of heavy rainfall are accounted for and cannot explain the trend.

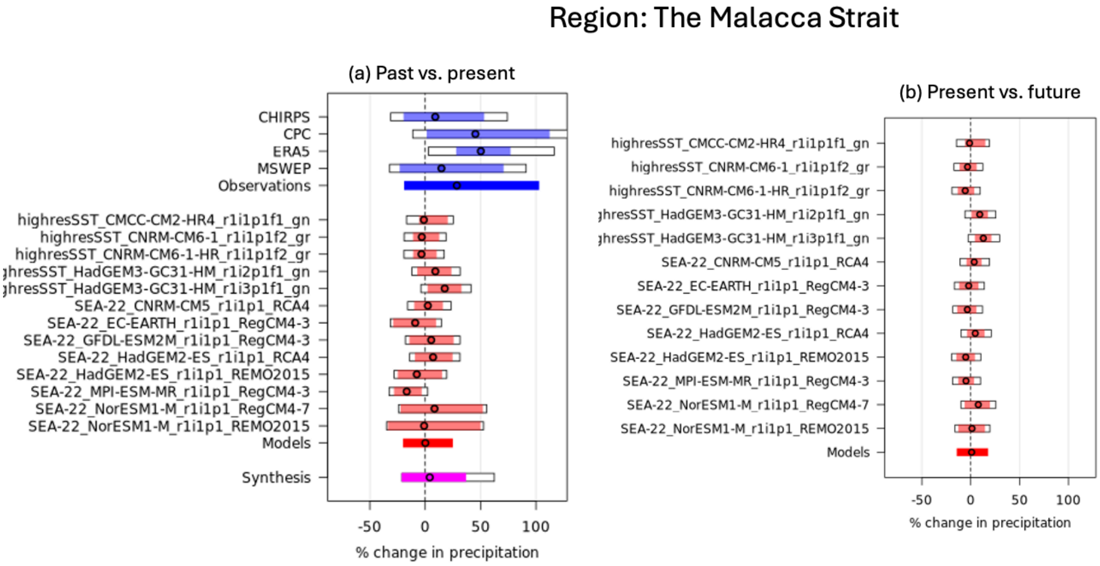

Figure 7.1 Change in intensity for Rx5day over the Malacca Strait region in % from past to present (left) and from present to future (right).

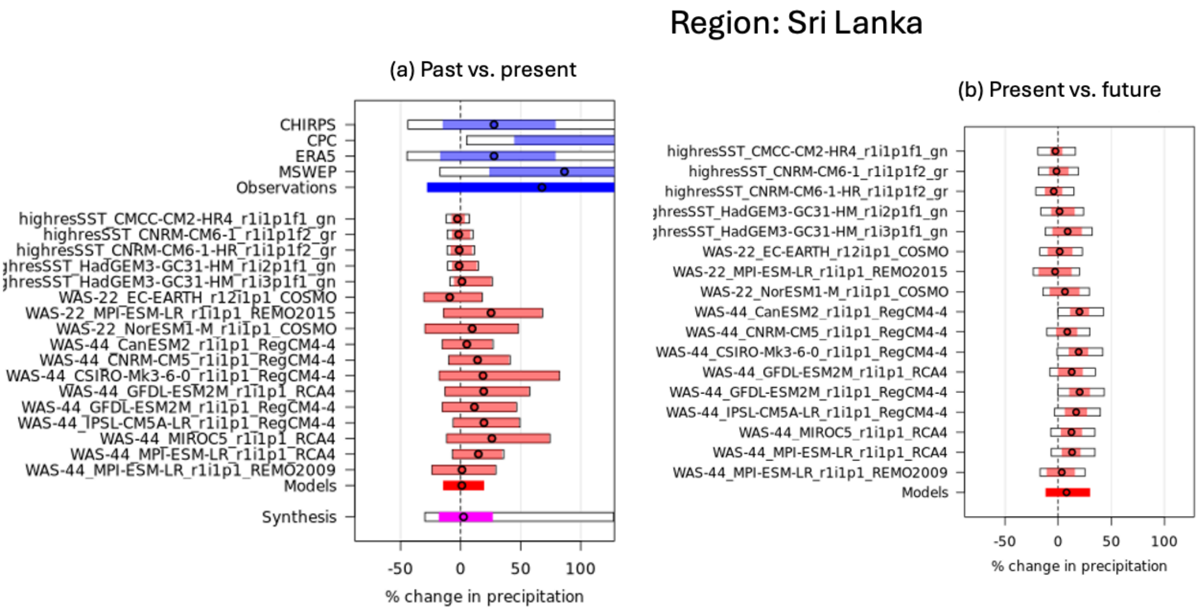

Figure 7.2 Change in intensity for Rx5day over Sri Lanka in % from past to present (left) and from present to future (right).

Data		Rx5day: Senyar	Rx5day: Ditwah
		Intensity change (%) (95% CI)	**Intensity change (%) (95% CI)**
Observations	**Past- Present**	28.528 (-15.012 to 98.745)	67.682 (-23.956 to 256.629)
Models		0.113 (-15.981 to 20.941)	1.01 (-10.579 to 15.531)
Synthesis		4.074 (-17.241 to 32.874)	2.388 (-14.185 to 22.714)
Models only	**Present- Future**	0.926 (-10.239 to 13.747)	7.842 (-7.838 to 25.989)

Table 7.1: *Summary of results for Tropical Cyclones Senyar over the Malacca Strait region and Ditwah over Sri Lanka, presented in Figs 5.1&5.2: changes due to GMST include past-present changes and present-future changes.*

8 Vulnerability and exposure

Sri Lanka's flood risk stems from its steep central highlands and low-lying coastal plains. Intense rainfall quickly channels runoff from the hills into crowded floodplains. In Indonesia, it is shaped by its vast archipelago of volcanic islands, broad plains, and deltas. With many islands having limited natural drainage and deep valleys, heavy rainfall easily triggers both flash floods and landslides.

These physical conditions framed the severe November-December 2025 floods. In Sri Lanka, Cyclonic Storm Ditwah became the deadliest weather-related disaster since the 2004 tsunami. The floods and landslides affected over 1.4 million people and displaced more than 233,000 across all districts. Across the North-East to central highland areas, some districts remain completely submerged or isolated by landslides at the time of writing. The Sri Lankan Disaster Management Centre estimates that almost 1,300 homes are completely destroyed with an additional 44,500 partially damaged in the region (Tamil Guardian, 2025). The disaster killed hundreds, inundated thousands of homes, and severely damaged infrastructure. The cyclone has impacted regions that drive more than 80% of the country's GDP, including manufacturing, financial and logistic sectors for an estimated loss of between Rs. 210 billion and Rs. 320 billion (Tamil Guardian, 2025).

In Indonesia, the arrival of Cyclonic Storm Senyar added a dimension of surprise. Senyar made landfall in northern Sumatra, an area rarely hit by cyclones. Heavy rain brought over a month's rainfall in a day to parts of Sumatra (with some areas receiving up to 400 mm), triggering flash floods and landslides in provinces like North Sumatra, West Sumatra, and Aceh - affecting more than 3.3 million people and causing hundreds deaths. Cyclonic Storm Senyar is the first significant extreme weather event since the large-scale flash floods and landslides due to monsoon during December 2006, which affected over 500,000 people across seven Acehnese districts (World Bank, 2006) and 400,000 in North Sumatra (ECHO, 2007), causing 47 deaths, massive displacement, destruction of thousands of homes, and an estimated US$210 million in economic losses concentrated in infrastructure, housing, and agriculture (World Bank, 2006). All these three regions have also inherited residual risk or accumulated legacy conditions (National Academies, 2022) from large-scale geological hazards over the past two decades, including an earthquake that hit North Sumatra in 2005, and devastating earthquakes that shattered West Sumatra in 2009. The most detrimental event was the Indian Ocean tsunami of 2004. Sri Lanka and Indonesia were severely affected with loss of life, damage to property, and infrastructure. The scale of damage in the tsunami resulted in massive displacements and recovery processes included relocation. Disasters push back years of development progress and recovery may remain insufficient (Fernando et al., 2025).

Further, recurring disasters, conflict, and recent impacts of COVID-19 pandemic, combined with economic crises, push vulnerable communities into debt traps and poverty. This makes recovery harder and re-creates risk and more vulnerability. The devastation from the Tropical Cyclones Ditwah and Senyar are indeed not a result of only the physical hazard, but also the exposure of people and assets to that hazard, and their vulnerability. Therefore, this section is a rapid analysis of vulnerability and exposure factors that both may have contributed to impacts, or helped avoid them. We focus on Sri Lanka and Indonesia, due to the unprecedented nature of the storms there. Given this is a rapid analysis, the full extent of the impacts of the storms are likely to only become clear in the weeks that follow, once emergency response teams can reach and survey areas that are currently unreachable and communications networks have been restored. Storm impacts can take even longer to fully unfold, as several health issues often appear only months to years after the event, including mental health, non-communicable diseases, and developmental impairments in children (Butsch et al., 2023).

8.1 Health

Sri Lanka

Sri Lanka's public health system is quite strong, providing nearly 95% of inpatient care and around 50% of outpatient care, prioritizing primary health care (WHO, 2021). The country has been able to eliminate malaria, filariasis, leprosy, polio and neonatal tetanus and achieve near elimination of most other vaccine-preventable diseases (WHO, 2021). However, vector-borne diseases remain a significant burden on public health, particularly in comparison to other infectious diseases; dengue fever is the most common with an incidence rate of 407.5 cases per 100,000 people in 2023 (WHO, 2024). In relation to gaps within the health system, geographical coverage still remains a challenge in remote areas in terms of infrastructure and staff (WHO, 2021). There is also the need to work on the health system's resilience and preparedness (WHO, 2021).

However, Cyclonic Storm Ditwah has deeply impacted Sri Lanka's health infrastructure. It is estimated that in all 25 districts, health services delivery had been affected to different degrees. For instance, a considerable number of Divisional Hospitals and Primary Medical Care Units across the flood-prone districts of Gampaha, Colombo, and Puttalam have sustained damage, including collapsed roofs, partially flooded wards filled with debris, and partial or complete loss of electricity and water (Disaster Management Centre of Sri Lanka, 2025). In addition, some hospitals are overcrowded, with some patients being airlifted to Colombo for urgent medical care (IOM, 2025).

The disruption of services, damaged facilities, and displacement have increased the risks of unassisted deliveries, pregnancy complications, and limited access to family-planning services (Disaster Management Centre of Sri Lanka, 2025). Vulnerable groups, such as under-five children, pregnant women, lactating mothers, people with disabilities and the elderly, face heightened risks of malnutrition as regular diet intake and supplementary nutrition sources are disrupted due to supply chain interruptions (Disaster Management Centre of Sri Lanka, 2025). According to an IOM report, immediate humanitarian needs include WASH assistance (clean water, sanitation, hygiene, sanitary kits), emergency health and trauma care, medicines provision, and MHPSS support for affected communities and responders (IOM, 2025).

WHO has warned that there is a significant risk of escalation of health risks like vector-borne, food-borne, water-borne diseases and food insecurity (UN News, 2025).

Indonesia

Health services in Indonesia are provided by the public and private sector, mostly undertaken by public services at provincial and district levels (WHO, 2017). Some of the main gaps in health systems are related to disparities between regions, including remote areas with limited access to primary care and specialized services (WHO, 2017). The country is impacted by dengue in 514 districts of urban and rural areas, where the disease has the highest disability-adjusted life years rate within Asia (Beacon, 2025). Chikungunya outbreaks have also been reported sporadically across the country and malaria remains an important infectious disease, especially in remote areas in eastern Indonesia (Marina et al, 2022).

Since 2014, Indonesia's Jaminan Kesehatan Nasional (JKN) has expanded health insurance coverage to over 98% of the population, including poor households through subsidised premiums. Despite this achievement, challenges persist. Financial sustainability remains uncertain as revenues and subsidies lag behind rising utilization and chronic, climate-sensitive disease burdens (Susilo et al., 2025). Geographic and socioeconomic disparities limit access and quality, especially in remote regions with shortages of health workers and weak primary care. Benefit design and payment systems favor hospital-based care over preventive services critical for climate-related risks. Fragmented governance further complicates integration of climate resilience into health financing and service delivery.

Sumatra overall has been prone to forest fire during dry seasons. During the 2015 El Niño year, many parts of Sumatra experienced dangerously high levels of sustained haze, with some areas exposed for up to two months (Lassa, 2015). Study suggests that there is a strong link of respiratory health to land-cover and climate changes. Drawing on 18 years of healthcare visit data for respiratory illnesses across Sumatran regencies (and other regions), researchers examine associations with rainfall variability, El Niño-driven drought, land-cover change, and fire events (Santika et al., 2023). Findings suggest that respiratory disease prevalence in Sumatra rose by approximately 8.5% during dry years, particularly in deforested peatland areas, and project further health risks under ongoing land-use and climate change.

A recent review on the impact of climate change on child nutrition in Indonesia suggests that there is adequate evidence on how climate variability and hazards (floods, droughts, fires, heat) affect child nutrition via food security, infections and health service disruption. There is a significant overlapping hotspots of climate and nutrition risk, drawing on district-level mapping in West Sumatra and parts of Aceh (Colozza et al., 2025).

Following the Northeast Monsoon and Cyclonic Storm Senyar making landfall in Indonesia, the Ministry of Health have established emergency health posts and temporary field hospitals to deliver health services to treat injured residents affected by the flooding and landslides (Jakarta Daily, 2025). This measure was taken after the damage of a considerable number of health infrastructure like hospitals and community health centers (Pukesmas) (Tempo, 2025).

The Ministry also warned the population to be alert to post-flood diseases, including leptospirosis and diarrhea, which commonly appear after large-scale flooding (Jakarta Daily, 2025). In addition, women and girls continue to face barriers in accessing proper sanitation, reproductive health services, increasing risk of illness, infection, and unplanned pregnancies (Plan International, 2025). Mental health is also impacted in these communities and the government has been providing psychosocial support across Sumatra to support disaster-hit residents cope with trauma and stress during the emergency and recovery periods (Antara News, 2025).

Given the scale of flash floods and landslides affecting 51 districts and cities in Sumatra, a major concern is the disruption of health services and supply chains. Vulnerable groups, such as people living with HIV, are likely to face interruptions in ARV supplies. Services for reproductive health and antenatal care for women have also been compromised. This situation illustrates how extreme weather events can severely undermine local health systems, increasing the risk of disease outbreaks in evacuation areas. Limited access to clean water further exacerbates public health challenges (UNOCHA, 2025).

8.2 Land-use changes

Sri Lanka

With nearly one-third of Sri Lanka's population depending on agriculture for their livelihood, the impact of recent floods has been devastating. Over 137,000 acres of farmland has been destroyed and critical infrastructure, such as dams and canals, have been damaged (NY Times, 2025). For a county where farming sustains millions, flooding poses a significant threat to both income and food security.

Policies and land-use practices in Sri Lanka have significantly influenced flood risk, particularly in the southwestern river basins. Flooding is the leading contribution to average annual disaster-related losses in Sri Lanka, with estimated damages reaching around USD $ 140 million each year (Climate Risk Country Profile: Sri Lanka (2020): The World Bank Group and the Asian Development Bank).

In the Gin River Basin, a flood-prone area in the Southern Provinces, land-use projections indicate that by 2050, agricultural lands will shrink to 17.5% whilst urban areas and shrubland will expand by 2.75% and 3.15% in the downstream areas of the basin (Jayapadma et al. 2024). A study by Maheng et al., 2019 has found that urban areas increased by approximately 51% between 1997 and 2015, resulting in the loss of numerous marshland and wetlands surrounding the city of Colombo.

Forest cover, which was about 90% in 1900, has declined to less than 20% by 2002 (Mapa et al., 2002). Recent deforestation and forest degradation in Sri Lanka are driven by a variety of scattered activities. Key drivers include slow encroachments for plantation crops (tea, rubber, coconut), cinnamon cultivation, at the forest fringes, infrastructure development projects, as well as illicit timber felling. These processes are fuelled by underlying factors such as rising local demand for timber, global market pressure for export crops, and commercialisation of rural economies (Fernando et al., 2015).

Combined with intensified rainfall during the monsoon season, the loss of forest and riparian vegetation diminishes floodplain roughness, accelerating runoff and exacerbating flood peaks, whereas the growth in built-up areas contributes to the increase of impervious surfaces which further heightens flood risk.

Indonesia

Data on forest cover change indicates that the three provinces affected by Cyclone Senyar - Aceh, North Sumatra, and West Sumatra - have been experiencing significant land-use changes (See Global Forest Watch). In particular, Indonesia is exposed to significant deforestation. Between 1991 and 2020, the country has lost 25% of its old growth forests with palm oil production contributing substantially to forest loss (Parker et al., 2024). Other drivers of deforestation include timber plantations, conversion to grasslands, logging roads and mining activities. Small-scale agriculture and plantations contributed to one fifth of deforestation occurring between 2001 and 2016 (Austin et al., 2019). Looking at total tree cover loss between 2001 and 2024, Indonesia lost 32 million ha of tree cover, representing 20% decline compared to 2000 levels (Global Forest Watch), resulting in a loss of protective barrier against floods.

Sumatra is one of the regions with highest deforestation rates (Global Forest Watch). By 2020, Sumatra was left without nearly half of its 1990 levels of primary forest area (Parker et al., 2024). From 2002 to 2024, Sumatera Barat (West Sumatra) lost 320,000 hectares of humid primary forest, representing 44% of its total tree cover loss. The humid primary forest area declined by 14%. Between 2001 and 2024, the province lost 740,000 hectares of tree cover, equivalent to 19% of its 2000 tree cover, and emitted 490 million tonnes of CO_2e. Similarly, between 2002 and 2024, Sumatera Utara (North Sumatra) lost 390,000 hectares of humid primary forest, making up 25% of its total tree cover loss. The humid primary forest area decreased by 19%. From 2001 to 2024, the province lost 1.6 million hectares of tree cover - 28% of its 2000 tree cover - resulting in 810 million tonnes of CO_2e emissions. Following cyclone Senyar, a large amount of logs have been swept into flood-hit residential areas in North Sumatra.

Sumatra is a strategically important island, ranking as the world's sixth largest at 470,000 km^2. It is a biodiversity hotspot with over 15,000 known plant species and more than 400 newly identified since 1995. However, the high forest loss poses severe risks to its unique ecosystems. Flash floods and landslides threaten hundreds of mammal species and other biodiversity, including critically endangered wildlife such as Sumatran rhinos and Sumatran tigers. The island also hosts the smallest Asian elephant and the highly threatened Sumatran orangutan (WWF, n.d.).

Aceh has also lost a significant share of its tree cover. Between 2002 and 2024, Aceh lost 320,000 hectares of humid primary forest, accounting for 38% of its total tree cover loss during this period.

The province's humid primary forest area decreased by 9%. From 2001 to 2024, Aceh lost 860,000 hectares of tree cover - 17% of its 2000 tree cover - resulting in 530 million tonnes of CO_2e emissions.

Deforestation significantly exacerbates impacts of cyclones by reducing slope stability and natural water retention, thereby intensifying the floods and landslides that commonly follow extreme storm events. Experts, as well as the environmental minister of Indonesia, have acknowledged that deforestation and environmental degradation contributed significantly to the severity of the disaster's impacts (Nindita et al., 2025). Research also suggests that in Sumatra, deforestation is driving the spread of dengue fever. For every 1% increase in forest cover, Husnina et al. (2019) recorded a 9% decline in the disease.

Today, Indonesia's forests cover 191 million hectares in total, out of which 63% is state forest, further divided into production forest (57%), protection forest (25%) and conservation forest (18%). Forestry and agriculture are 34% of Indonesia's GDP. Although this has brought economic development, it also came with many social and environmental costs, including alarming rates of forest loss. Indonesia's recent policy reforms, including the now-permanent moratorium on new forest concessions, aim to protect forests while also improving food security, reducing rural poverty, creating a more efficient and less fragmented agriculture sector, promoting sustainable use of productive forests, and strengthening environmental conservation (FAO, 2020).

8.3 Urban planning and informality

At a global scale, floodplains are being altered at a substantial rate, the number of people living in flood-prone and urban regions is growing faster than the number living in other regions. A quarter of the fastest growing cities in the last decade are in Central and Southern Asia (UN DESA, 2025). Across South and Southeast Asia, rapid urbanization, settlement in low-lying floodplains and deltas, and high population densities in coastal areas have created very large concentrations of people and assets exposed to fluvial, pluvial and coastal flooding (Rogers, 2025). Disasters are closely linked to developmental processes (Raju, Boyd & Otto, 2022). Urban growth and land-use changes have increased risks through soil sealing, impacting drainage of floodwaters with consequent sewer overflows and surface runoff, reducing drainage capacity and worsening flood impacts on city infrastructure (IPCC, 2022).

Across the two countries, a significant share of the population - 14–20% in some national assessments - lives in high-intensity flood-risk zones, with critical infrastructure such as roads, railways, and cropland also concentrated in these areas. Rapid urbanization in deltas and coastal plains, expansion of settlements into marginal hillslopes, and infrastructure built in or near frequently flooded corridors have collectively elevated exposure to these flood events (Rentschler, 2022).

As a result, both countries have a high baseline vulnerability and exposure, shaped by not only concentration of people but also cascading failures of transport, power and basic services, the prevalence of informal or substandard housing, and gaps in risk-informed land-use planning and enforcement. These structural factors, combined with socio-economic inequalities, limited savings and insurance coverage, and varying access to early warning information, safe evacuation routes and social protection, mean that low-income households, residents of informal settlements and marginalized groups bear a disproportionate share of damages and losses from the ongoing floods

(World Bank, 2023).

Indonesia

A similar impact on urban infrastructure occurred in Indonesia. Dense settlement in flood-prone lowlands and along riverbanks - especially in parts of Sumatra and other affected islands - places large urban and peri-urban populations directly in the path of river and surface flooding. Steep, erosion-prone hillsides that have been cleared or developed for housing and agriculture further expose communities to landslides and debris flows triggered by extreme rainfall (Prevention Web, 2025). However, the Indonesia government has communicated a reforestation plan at COP29, aiming to reforest 12.7 million hectares of degraded land (Mongabay, 2024). Key transmission towers collapsed during flash floods, triggering widespread power outages and hindering emergency response. Flooding in towns such as Idi Town (East Aceh) destroyed roads, public facilities, shops, and homes, isolating communities and causing outages in electricity, water, and internet services. Major roadways including the Tarutung-Sibolga Road were paralyzed by floods and landslides, severing transport routes critical for relief and supplies. Damage to public infrastructure like government buildings, religious sites, educational institutions, and bridges was extensive, further disrupting daily urban functions (Human Initiative, 2025).

Sri Lanka

The disruption of services and substantial damage to urban infrastructure in Sri Lanka is not much different than in Indonesia. Major concentrations of people and assets lie in flood-prone river basins and low-lying urban areas, including around Colombo and interior provinces where river overflows and ponding inundate neighbourhoods and services (GFDRR, 2018; Dmdok & Kakm, 2021). Limited maintenance of drainage worsened inundation in peri-urban areas, affecting over 1.5 million people and key services. Severe flooding along the Kelani River in Colombo submerged roads, disrupted railway sections, and caused damage to over 10 bridges, hampering urban mobility and connectivity (UN News, 2025). The national power grid was affected, causing electricity outages for large urban populations; telecommunications and internet were also disrupted, and the scale of infrastructure damage was severe enough to strain emergency response capabilities and prolong the recovery period. Some neighbourhoods in Sammanthurai in east central Sri Lanka are completely buried under mud (UN-OCHA, 2025, Al Jazeera, 2025).

More than 137,000 acres of agricultural land are said to be destroyed by the floods, in parts also due to destroyed dams and canals. This destruction came a few weeks after rice paddies had been planted. This loss is particularly detrimental for the one-fourth of Sri Lanka's population which makes a living from agriculture (Department of Census and Statistics, 2023; FAO, n.d.).

8.4 Insurance

Lack of adequate insurance coverage is one of the main drivers of vulnerability not only to floods but all kinds of disasters and shocks (The World Bank, 2025). It constrains recovery for low-income and informal workers and increases long-term socio-economic impacts from repeated extreme rainfall and flood events. The insurance industry now classifies cyclones and other extreme weather 'structural risk drivers'. Flood insurance is often risk-based, which leaves many informal and poor households without coverage because it is too expensive or inaccessible. The problem is aggravated by a general lack of trust in the insurance industry and limited understanding of policies overall (Oxford Business

Group, 2019). Public and private insurance in Indonesia and Sri Lanka is limited in protecting the most vulnerable households from flood losses. Some social insurance and ad-hoc disaster support measures partially cushion impacts, especially for formal workers. Overall disaster risk insurance coverage is low and large portions of damage to homes, small businesses and informal livelihoods are effectively uninsured in all three countries (OECD, 2025).

These gaps in insurance coverage mean that poorer and informal households absorb most flood-related losses themselves, increasing their dependence on social protection programs. Currently, only 41.3% of the population is covered by at least one social protection program. However, the country had demonstrated it's ability to scale up social protection for shocks during the COVID-19 pandemic to protect the most vulnerable groups against income shocks through cash top-ups in their Samurdhi (ILO, 2025; Batawala, 2025).

Indonesia

Indonesia has a growing but still limited non-life insurance sector, with some coverage for businesses and better-off households. Only about 3 percent of micro, small, and medium enterprises (MSMEs) have disaster insurance while household flood coverage is less than 10%. Only residential earthquake insurance policies exist with penetration less than 1%. This leaves many homes and small businesses in high-risk areas uninsured and relies on government relief, donor assistance, and credit moratoria after disasters. Private non-life insurance exists voluntarily for assets and businesses, but flood-specific coverage is shallow (<10% household penetration) and risk-based, excluding many informal/rural homes. There is no national flood pool (OJK, 2020).

Maipark, Indonesia's leading catastrophe reinsurer, reports that residential catastrophe insurance penetration averaged just 0.0028% of GDP between 2018 and 2022, while earthquake coverage accounted for an annual average of 3.8% of insured losses. Residential earthquake policies in force averaged only 107,000 per year nationwide. Established as a mandatory earthquake pool, Maipark has evolved into a hybrid reinsurer and emerging climate-risk hub, prioritizing seismic coverage but offering optional add-ons for floods and parametric weather risks, though uptake remains minimal. Most climate-related losses especially floods, droughts, extreme rainfall, remain largely uninsured, with limited coverage under pilot parametric schemes for agriculture and weather risk (Indirazkia & Atmaja, 2024)

Sri Lanka

Sri Lanka operates national schemes for social security and health insurance for parts of the population, but coverage of specific flood or property insurance products is limited, particularly for poorer households and small farmers in flood-prone river basins and landslide-prone hills. Additionally, the flood insurance program introduced by the government in 2016 and 2017 is not functioning anymore because of the insufficient funds allocated to execute such assistance programs (Ashvini, 2025). Social security and limited private property insurance apply, but dedicated flood coverage is voluntary, low-penetration, and urban-focused; small farmers/homes largely uninsured. Claims handled by private insurers or national schemes with post-disaster grants/loans as primary recourse. Following major disasters, the financial burden of repairing homes, replacing assets and restoring livelihoods typically falls on affected households, supplemented by government relief grants, concessional loans and international assistance rather than pre-arranged insurance payouts

(Ashvini, 2025). Finally, experts state that the effective pricing of policies is impeded due to limited access to loss and damage data.

8.5 Governance

Sri Lanka

Sri Lanka has been facing complex political and economical challenges over the last decade, accompanied by a series of deadly Jihadist terrorist attacks between 2015-2019. Marked by an almost three decade-long civil war between 1983-2009, continue to shape social incohesion and inequalities as well as marginalization of certain population groups based on geographic, ethnoreligious and linguistic characteristics remains persistent (Anandakugan, 2020; BTI, 2024). Language barriers seem to be an obstacle in the current humanitarian response as official communication has not been conducted in all languages spoken in the country (DW, 2025). Recurring extreme weather events, especially flooding, regularly lead to the displacement of population groups within the country, with an estimate of 3.5 million individuals having been displaced between 2008-2024 (iDMC, 2024). Additionally, the civil war led to an internally displaced population which to some degree still remains displaced today (iDMC, 2024).

The country has not fully recovered from an economic crash in 2022. The crisis was the result of a reduction in government revenue due to tax cuts and increased government spending as well as a lack of foreign trade and currency to import necessities such as fuel (BTI, 2024). In addition, the country did not interest payments on its foreign debt for the first time in 2022 (Sharma et al., 2022), also due to external shocks such as the Covid-19 pandemic (BTI, 2024). This led to a stark increase in petrol and diesel prices, power cuts and a public transportation network collapse (George & Baskar, 2022; BBC, 2023) as well as a shortage of medicine and other essentials (Matthias & Jayasinghe, 2022). The inflation rate rose to 50% (Sharma et al., 2022), resulting in a humanitarian crisis as well as a political uprising. The International Monetary Fund (IMF) agreed to support subsequent economic policies and reforms to counteract the economic recession (IMF, 2023). Still, the country's poverty rate has doubled since 2022 to 24.5% in 2024 (World Bank Group, 2025) and could increase a further 10% by the cyclone's economic impacts, as stated by officials (NYT, 2025b).

In addition, Sri Lanka experiences recurring annual floods, which further impact GDP growth and thus economic and societal development (Fernando et al., 2023). Administrative structures used to provide essential services, such as health and educational services, have been highly politicized and show an overall deterioration, for example through the emigration of health care professionals (BTI, 2024).

In this context, the country is currently requesting international aid to finance relief and reconstruction activities and will set up a public-private recovery fund (NYT, 2025, economynext, 2025). The government of Sri Lanka declared a nationwide state of emergency as well as the Essential Public Service Act No. 61 on November 28 which grants the government broad powers to ensure the continuation of essential services (IFRC, 2025). The World Bank is supporting these efforts with a Global Rapid Post-Disaster Damage Estimation (GRADE) to estimate the economic impacts of the storm (economynext, 2025), as requested by the Sri Lankan government. The overall international aid response is limited by funding constraints, especially in light of the recent financial cuts of different governments.

Indonesia

Following the democratic transition in 1998, population displacement increased significantly. For example, in 2002, a reported 1.4 million people were internally displaced (SIDA, 2004). Between 2010–2021, 6.5 million new displacements were linked to over 1800 disaster events recorded across the country. Floods accounted for 63% of the displacements, earthquakes for 21%, and volcanic eruptions for 13%. Storms and wet mass movement, such as landslides, accounted for the rest (iDMC, 2023)

In Indonesia, 10% of people live below five meters above sea level (IEP, 2022) signalling an expected increase in internal migration (Kulp, 2020). Hazard maps show that a significant proportion of the population lives in areas of high risk. More than 11 million people live in areas prone to earthquakes, and around 2.5 million people are exposed to tsunamis (iDMC, 2023). For example, in 2022, over 300 000 people in Indonesia were displaced due to typhoons, floods, storms and earthquakes (IOM, 2024)

Since the 2004 Tsunami, Indonesia has focused on a nationally-driven coordinated response and finance mechanisms for disaster response and humanitarian support (Byrant, 2025). The country has developed comprehensive policies on disaster displacement and dedicates significant public resources to their implementation(iDMC, 2023).

8.6 Flood risk management

Sri Lanka

Sri Lanka has an operational national early warning system (EWS) that is a multi-hazards system involving tsunami, cyclones, floods, landslides and sea surges (CFE-DM, 2024). The EWS comprises technical agencies responsible for hazard monitoring and analysis, and for dissemination of information products and warnings. According to the national Disaster Management policy, the Department of Meteorology monitors meteorological and tsunami hazards, the National Building Research Organization (NBRO) is in charge of landslides hazards, the Geological Survey and Mines Bureau for seismic hazards, the Department of Coast Conservation (NARA) for coastal and sea level hazards, the Department of Irrigation for river flooding, the Land Reclamation and Development Corporation for storm drainage and urban flooding, and the Ministry of Health for health-related hazards (CFE-DM, 2024). The EWS is coordinated by the Disaster Management Centre (DMC) which links technical agencies and local authorities to issue and disseminate warnings, and coordinates and runs emergency operations as well as early warning services. The national EWS is complemented by the Regional Integrated Multi-Hazard Early Warning System for Africa and Asia (RIMES) which generates and communicates early warning information and develops regional capacity to prepare for and respond to trans-boundary hazards for 48 member and collaborating states.

In general, the performance of the national EWS varies by hazard, location, and lead time. As mentioned before, the flood EWS involves multiple agencies combining meteorological forecasting from DoM, hydrological monitoring and flood warnings for riverine floods and dam/reservoir related flood risk, the issue of alerts and warnings, their communication and dissemination as well as institutional coordination by the DMC and the public-information dissemination networks. Hydrological/river forecasts often provide hours to a few days lead time depending on basin size, station density and upstream rainfall forecasts while general weather forecasts provide up to 7 days of advance notice for heavy rainfall events.

Early morning on 28 November 2025, Cyclone Ditwah made landfall in Sri Lanka resulting in devastating nationwide floods. On 29 November, the government activated the Union Civil Protection Mechanism (UCPM) for search and relief operations. Before these catastrophic flooding events, the DMC started issuing continuous alerts, advisories and public warnings following NBRO reports and the steadily increasing rainfall since 18 November. These were disseminated through the DMC and DoM official websites and social media, national media (radio/TV), municipal disaster units, DMC emergency hotlines, early-warning towers/sirens in some zones, NGOs, community-based organizations, volunteers as well as via SMS/text and other digital channels. The use of such diversified communication and dissemination channels allows the information to reach many people including the last mile communities, however alerts and following updates were not disseminated equally across all official languages, with majority of in Sinhala, some in English and rarely in Tamil (Hippola et al., 2019; Jayasekara, 2021, Krishnan, 2025). There have also been reports on communication breakdowns, due in part to infrastructural failure of telecommunications towers (The Morning, 2025).

Despite the multi-agency coordination and the wide range of communication and dissemination channels, there are still some limitations and gaps in flood EWS. For instance, there are still uncertainties in the flood forecast and the accuracy varies according to the locations depending on the availability of monitoring stations. In addition, there is a lack of application of adequate flood models which contributes to poor understanding of the potential impacts and need for timely action.

Since the communication and dissemination channels rely importantly on institutions, mobile applications and media networks, people in rural/remote areas and marginalized communities with low adoption of these dedicated channels have sometimes limited access to warnings or receive them with little lead time (Hippola et al., 2019; Jayasekara et al., 2021).

Many efforts have been made in terms of using structural measures to reduce flood risk in Sri Lanka. These include the construction of reservoirs, dams and storage systems to regulate water flow, the urban drainage infrastructure and pumping stations (eg. Ambatale Pumping Station that helps to drain stormwater during heavy rains instead of letting it accumulate) and the use of nature-based solutions such as the restoration of wetlands. However, none of these structural measures could withstand the magnitude of the floods brought by Cyclone Ditwah.

Recognizing the need to shift from traditional to proactive response to disasters, the government of Sri Lanka, through the DMC, launched its first pilot projects in 2022 to test anticipatory action (AA) approaches for floods and landslides in Nuwara Eliya (Anticipation Hub, 2025). There are now many more AA initiatives across the country, including at community level and for a range of hazards. In 2025, the AWARE (Early Warning - Early Action - Early Finance) platform (Alahacoon & Amarnath, 2023) was launched by the International Water Management Institute (IWMI), in partnership with the DMC and other humanitarian and government actors, to strengthen coordination between forecasts, early warnings, anticipatory planning (pre-positioning, evacuation, support) and financing for vulnerable communities. The platform aims to institutionalize early-action mechanisms, making the link between forecast-based alerts and concrete funded preparatory measures (evacuation, resource prepositioning, cash transfers, etc.). Additionally, the NBRO hosts a data sharing platform to increase stakeholder collaboration for landslide risks (see NBRO, n.d.) However, experts state that while good intentions underlie these efforts, they are often ineffective in reality due to entrenched situational biases to full scale cooperation and coproduction of solutions with all stakeholders.

Ahead of floods, the government undertook actions, including the communication and dissemination of early warnings as well as evacuation. The International Federation of Red Cross and Red Crescent Societies (IFRC) has provided vital technical and financial support to the Sri Lanka Red Cross Society (SLRCS), enabling the pre-positioning of essential stocks such as shelter materials, hygiene kits, and health supplies in high-risk areas.

After the floods hit the country, the government declared a state of emergency nationwide and the UN and humanitarian partners have activated a coordinated multi-sector response, begun a Joint Rapid Needs Assessment, and are developing a Joint Response Plan to guide relief and resource mobilization. The military (army, navy, air force), police and civil defense forces of 20,000 personnel were deployed to conduct search and rescue operations, evacuations (by boat, helicopter), assist stranded people, and reach isolated areas cut off by floods or landslides. The Sri Lanka Red Cross Society (SLRCS) mobilized more than 3,500 volunteers, to conduct rapid assessments, support evacuations, provide first aid, and distribute safe water, hygiene kits, bedding, and food rations. However, road closures and the risk of secondary landslides continue to hamper relief efforts. Apart from the aforementioned stakeholders, the private sector plays a major role in disaster risk management in Sri Lanka. For example, in February 2025, the Ceylon Chamber of Commerce (CCC) in collaboration with the DMC launched the Core Humanitarian Standards guideline (CCC, 2025a) to help the private sector respond ethically to climate-related disasters. Recall that the CCC is the apex representative of the private sector in Sri Lanka and consists of a strong network of industry associations, affiliations and sector expertise working in business promotion and trade facilitation, while contributing to national economic policy development. Following the recent flood in November 2025, the CCC initiated immediate humanitarian responses focusing on fund raising, donation collection and repurposing funds for immediate relief and long-term resilience building (see CCC, 2025b,c). Experts mention that bringing in private sector actors is hoped to improve cross-organizational collaboration and strengthen value chains.

Moreover, the government of Sri Lanka elaborated in 2020 its Contingent Emergency Response Component (CERC), a flexible financing tool, often used in World Bank Group projects, that allows governments to quickly access pre-approved funds to respond effectively to sudden, major crises like natural disasters, epidemics, or conflicts, ensuring immediate support for essential goods, services, and recovery without lengthy new approval processes. The government declared a state of emergency following the November 2025 floods (IOM, 2025) and the CERC was activated (World Bank, 2025; Adaderana, 2025). A state of disaster as per provisions in the 2005 Disaster Management Act was not proclaimed.

Indonesia

Disaster risk management (DRM) policy in Indonesia is governed by Law No. 24/2007, which established the National Disaster Management Agency (BNPB) to coordinate efforts and implement proactive measures. The Law led to the establishment of BNPB in 2008. This policy reform led to the establishment of more than 500 local disaster management offices at subnational levels (Sufri & Lassa, 2024). Since then, BNPB has played a key role in providing leadership and building local government capacity in areas such as promoting community-based programs in every village (Lessy et al., 2025) and ensuring each district/city develops contingency plans and early warning systems. Progress has been made, though it varies across regions.

Despite the fact that a multi-hazard early warning system (MHEWS) has been formally initiated, the system still faces integration challenges, as different ministries have different visions about MHEWS. For example, the Ministry of Communication and Informatics recently developed the National Early Warning System for Disasters (SNPDK), which consists of the Early Warning System (EWS) and the Disaster Prevention Information System (DPIS) (Setkab, 2025). The system's primary achievement has been the promotion of the digital ecosystem including digital broadcasting from Digital TV and SMS blast, radio, agency websites and social media, to transmit warning messages. Such a system has not yet been adequately evaluated.

The SNPDK is a polycentric system where there are many, at best, complementary and, at worst, overlapping and conflicting governance arrangements. The Meteorology, Climatology, and Geophysics Agency (BMKG) has a more mature hazard monitoring system and has been legally mandated to monitor weather, climate, and related hazards and provide early warning information for the country. In theory, the MHEWS platform managed by BNPB integrates BMKG forecasts with risk and exposure layers to generate impact-based information. River-basin flood early warning systems are managed by Balai Besar Wilayah Sungai (Large River Basin Authority) and local Public Works offices. So far, what is quite clear is that BMKG has also been the focal point for hydrometeorological hazard early warning systems. BMKG provides rainfall and cyclone forecasts, while the promise for impact-based EWS services from BNPB remains to be seen how it will be operationalised on a routine basis.

On 23 November 2025, high intensity rains began due to Tropical Cyclone Senyar, aggravated by unstable atmospheric conditions (IFRC, 2025). On 26 November 2026, Senyar made landfall in Indonesia causing devastating flooding and landslides in Sumatra, leading to hundreds of casualties and widespread damage across the country (IFRC, 2025; TDMRC, 2025; WMO, 2025). At the end of October 2025, the BMKG started issuing multiple warnings regarding the onset and peak of the rainy season, urging preparedness for extreme weather, high rainfall, and potential flooding and landslides across various Indonesian regions. Throughout November, specific alerts were issued for regions at risk. For example, in early November, BMKG warned of heavy rain potential in areas like North Sumatra and Central Java. By late November, following initial floods, they predicted that adverse weather and heavy rainfall would continue in the western and southern regions of North Sumatra until the end of the month.

Anticipatory action, initiated first in 2015 with pilot projects supported by the International Federation of Red Cross and Red Crescent Societies (IFRC), has grown significantly and is currently well integrated into the country's disaster management framework (WPF, 2025). The Palang Merah Indonesia (PMI, Indonesian Red Cross) completed its first "Early Action Protocol (EAP) for floods" with the support of IFRC in February 2025. As part of AA, the BNPB and local governments across several provinces had reportedly started pre-emptive measures ahead of the rainy/flood season by inspecting and preparing disaster-response infrastructure and logistics, reviewing flood-defense works (such as embankments and drainage), and urging local authorities to be on alert. The regional disaster office for Jakarta (the provincial BPBD) activated anticipatory measures for potential coastal/tidal flooding in early November 2025 by preparing for temporary evacuation if water levels exceeded thresholds (e.g. 50 cm), and enhancing monitoring and public communication. All these anticipatory actions taken ahead of the floods appeared to be insufficient to avoid the catastrophic impacts.

In response to widespread, cyclone-driven floods and landslides, the country's response actions involved coordinated efforts between government agencies, the military, national NGOs like PMI, and international aid organizations. The main actions are focused on search and rescue, aid distribution, and restoring essential services in affected provinces like Aceh, North Sumatra, and West Sumatra. PMI has mobilized staff and volunteers to conduct evacuations, provide First Aid, distribute clean water, and operate public kitchens, but access remains difficult and resources are stretched.

Communication breakdown partially due to infrastructural failure of telecommunication towers but also to unknown reasons, still trying to restore. Technological capacities need to be strengthened overall.

V&E Conclusions

The floods associated with Cyclones Ditwah in Sri Lanka and Senyar in Indonesia illustrate how natural hazards intersect with patterns of development, land-use change, and differential vulnerabilities to shape impacts. In both countries, decades of rapid urbanization and high concentration of people, infrastructure, and critical services in low-lying floodplains and deltas heightened exposure to extreme rainfall. In Colombo and along the Kelani River (Sri Lanka), dense settlement and reduced drainage capacity worsened inundation and prolonged service disruptions, while in North and West Sumatra (Indonesia), communities along riverbanks and steep, erosion-prone hillsides experienced severe flash floods and landslides that cut off transport routes and power networks. In both contexts, extensive deforestation contributed to reduced slope stability and natural water retention, amplifying downstream flood peaks and debris flow. In Indonesia, however, environmental reforms - including the permanent moratorium on new forest concessions - represent important longer-term efforts to reduce risks linked to deforestation.

Across both countries, cascading failures of transport, energy, communications, and basic services disproportionately affected low-income and marginalized groups, who are more likely to live in informal or substandard housing and to lack savings or insurance. In Sri Lanka, entire neighborhoods in districts such as Sammanthurai were buried under mud, and damaged bridges and road closures hindered access to health care and emergency assistance. In Sumatra, Indonesia, the destruction of key transmission towers and local road networks left communities in Idi Town and other districts isolated for days.

The events also highlight challenges in flood risk management systems. Both governments issued warnings ahead of the cyclones, providing at least some lead time for early action. Sri Lanka's

MHEWS and its partnerships with regional platforms such as RIMES contributed to sustained monitoring and regular public advisories. Similarly, Indonesia's BMKG provided continuous weather updates and local governments in several provinces conducted pre-season inspections and checks of critical flood-defence infrastructure. Additionally, growing anticipatory action efforts - such as Sri Lanka's AWARE platform and Indonesia's Early Action Protocol for floods - signal important shifts towards more proactive disaster risk management. However, uncertainty in hydrological forecasts and limited application of impact-based models posed challenges to the roll-out of anticipatory action. In Sri Lanka, communication barriers - such as uneven dissemination of alerts across Sinhala, Tamil, and English languages - combined with telecommunications outages meant that some communities received warnings late or not at all. Emergency spillage from dams also contributed to downstream inundation, underscoring the complexity of managing competing water-use priorities during extreme rainfall. In Indonesia, weather and flood alerts were issued well in advance, but several challenges limited how useful they were for communities. Warnings came through different agencies and channels, which could create confusion about which messages to follow. In part of North and West Sumatra, the rainfall intensified very quickly, leaving residents and local authorities little time to act. Damage to power and communication towers further disrupted information flow at critical moments. However, in both countries, strong community networks and experience with past disasters helped some neighborhoods organize evacuations quickly and support isolated households during the first hours of the floods. Further, the role of volunteers - including Sri Lanka Red Cross and Indonesian Red Cross Society (PMI) - substantially supported early evacuations, first aid, and relief distribution.

It is important to note that this analysis is conducted in the immediate aftermath of the disasters, and based on the limited information available within this narrow and challenging window of time. On the one hand, access constraints, damaged communications networks, and ongoing response operations prohibit the completeness of reported impacts. On the other hand, many impacts, especially those related to health and livelihoods, will only fully materialize months to years after the event. Further, impact assessments, after-action reviews, and further research are essential to to capture the full scope of damages and losses, and assess the degree to which each factor played a role in the disasters.

In addition to the physical hazard, the impacts observed in Sri Lanka and Indonesia were shaped by where and how people live, the condition of ecosystems and infrastructure, and the ability of institutions to anticipate, communicate, and act at the speed required by rapid-onset and fast-evolving events.

9 Conclusions

The impacts related to extreme rainfall and flooding associated with storms Senyar and Ditwah were shaped by climate change, natural variability, rising sea surface temperatures and vulnerability. The tropical location of both regions means rainfall in the region is driven by several modes of variability including, but not limited to ENSO and IOD influences that were factored in this study. For example, an exceptionally active ITCZ and accompanying equatorial waves helped organize deep convection close to the equator, enabling slow-moving systems that produced prolonged, intense rainfall over both study regions. While La Niña and a negative IOD contributed to the intensity of the Malacca Strait event, observations across both regions show clear upward trends in the heaviest 5-day rainfall totals consistent with a warming climate. However, available climate models do not reproduce these trends and show no consistent direction of change, limiting our ability to quantify the influence of human-induced climate change on these events. Given the trends in the observations and the physical understanding of the climate, climate change is likely one driver of increasing intensity of extreme rainfall in these parts, although its exact contribution cannot yet be robustly assessed.

The severe impacts highlight how rapid urbanisation, high exposure of communities in flood-plains and vulnerabilities in infrastructure and early-warning amplify the risk. Together, these findings point to the need for strengthening climate resilience in these regions, to help adapt to future events.

Data availability

All time series used in the attribution analysis are available via the Climate Explorer.

References

All references are given as hyperlinks in the text.

Appendix

A.1 Additional details

National Flood Assessment: Inundation Extent Quantification

IWMI's rapid flood assessment (Fig. A1) shows that 10.79% of Sri Lanka's land area (7,120.8 km^2) was submerged after Cyclone Ditwah. The most affected areas were the low-lying agricultural and settlement zones of North Central, Eastern, Northern and North Western provinces, each experiencing roughly 13–18% inundation. These provinces form the flat central plains and northern corridor (e.g. Anuradhapura, Trincomalee, Vavuniya districts) that were especially vulnerable. The flood map was generated from satellite SAR data as of 26–28 Nov, using three co-registered sensors, and represents a preliminary inundation mask. The spatial pattern in Fig. A1 highlights that the national flood footprint was extensive, covering river basins like the Mahaweli, Deduru Oya, and Malwathu Oya as well as the Kelani valley, and affecting both rural and urban areas (e.g. greater Colombo).

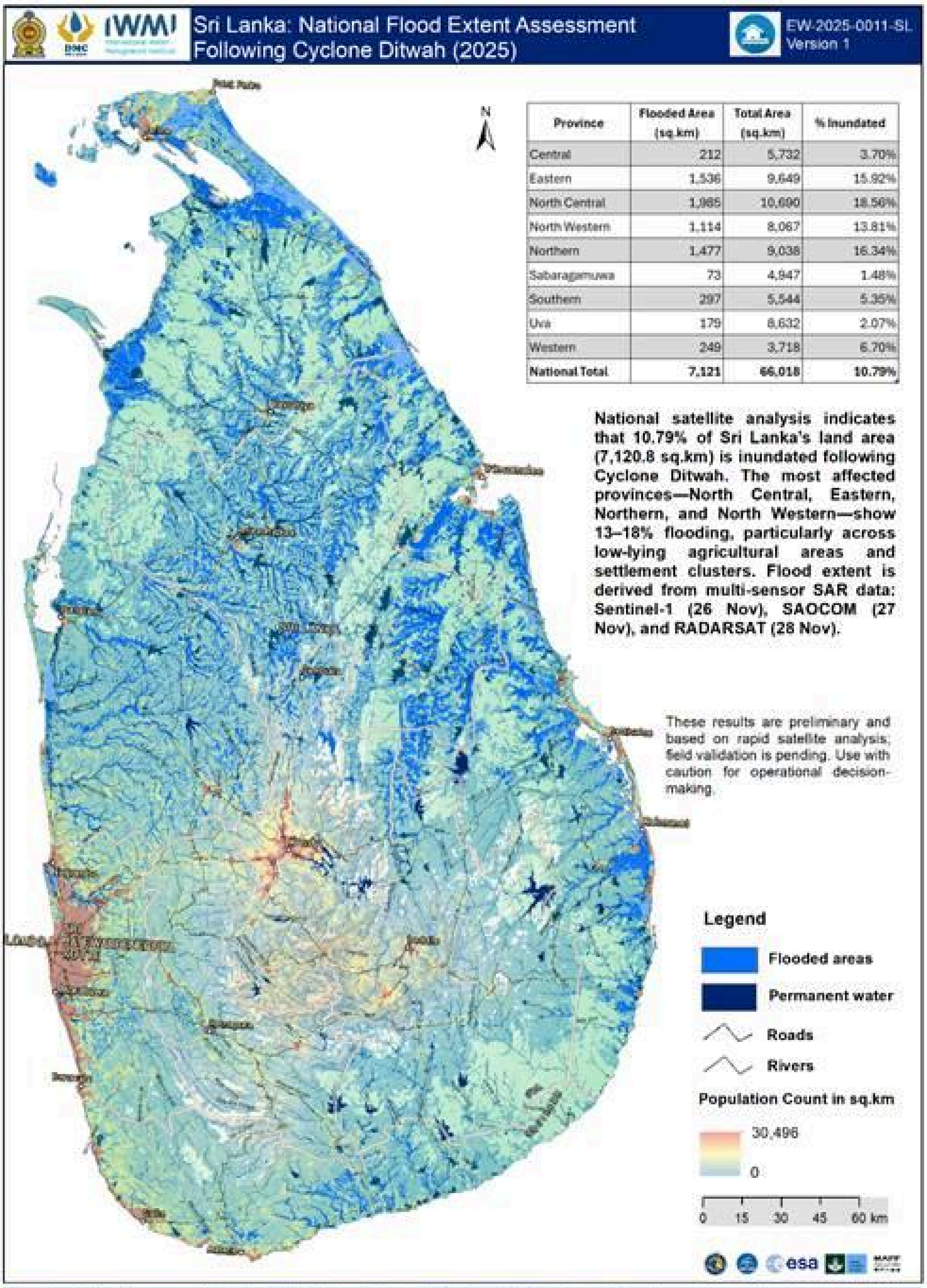

Figure A1: National flood inundation after Cyclone Ditwah (IWMI satellite analysis). Shading shows percent of land flooded by province. 10.79% of Sri Lanka's territory (≈7,120.8 km²) was inundated. North Central, Eastern, Northern, and North Western Provinces saw the highest flooding (13–18% of area). Flood extents were derived from multi-sensor SAR imagery (Sentinel-1 on 26 Nov, SAOCOM on 27 Nov, RADARSAT on 28 Nov).

The spatial distribution of the quantified inundation extent, presented in Table A1, confirms that the North Central Province was the most severely affected region, both in absolute area and percentage, with 1,985 sq.km (18.56% of provincial area) flooded.

Table A1: National Flood Extent Assessment Following Cyclonic Storm Ditwah (November 2025)

Province	Flooded Area (sq.km)	Total Area (sq.km)	Percentage Inundated
Central	212	5,732	3.70%
Eastern	1,536	9,649	15.92%
North Central	1,985	10,690	18.56%
North Western	1,114	8,067	13.81%
Northern	1,477	9,038	16.34%
Sabaragamuwa	73	4,947	1.48%
Southern	297	5,544	5.35%
Uva	179	8,632	2.07%
Western	249	3,718	6.70%
National Total	**7,121**	**66,018**	**10.79%**

Impact on Agricultural Production: Analysis of Flood-Affected Paddy Areas

The consequential flooding severely impacted the agricultural sector, particularly rice production, which is crucial for national food security and local economies. The total estimated area of flood-affected paddy land reached 601,972 acres.

The classification of flooded rice areas utilized a rigorous remote sensing technique involving pixel-wise VV/VH backscatter change detection applied to Sentinel-1 SAR pre- and during-flood imagery acquired on 26 November 2025. This specific method leverages the differences in co-polarized (VV) and cross-polarized (VH) radar returns to achieve high-fidelity differentiation among open water bodies, fully submerged vegetation, and partially saturated ground conditions. This detailed classification allowed the assessment to distinguish between fully and partially submerged paddy fields, providing robust and nuanced estimates of agricultural loss. Fig. A2 illustrates the spatial extent of paddy flooding. The analysis indicates particularly heavy damage to rice in the Paddy Triangle (Anuradhapura/Polonnaruwa in North Central Province) and the Chena paddy areas of the north and east. In such locations, flood depths likely exceeded 15–30 cm for 1–2 days or more, which can destroy standing rice. This confirms that the November floods struck Sri Lanka’s heartland rice zones hard, threatening food security and farmers’ incomes (consistent with reports of disrupted rice supplies and rising food needs).

The provincial distribution of paddy loss mirrored the general flood extent, confirming the concentrated vulnerability of major agricultural regions. The North Central Province recorded the highest loss at 160,654 acres, followed closely by the Eastern Province (138,952 acres), North Western Province (108,829 acres), and Northern Province (106,195 acres) (Table A2).

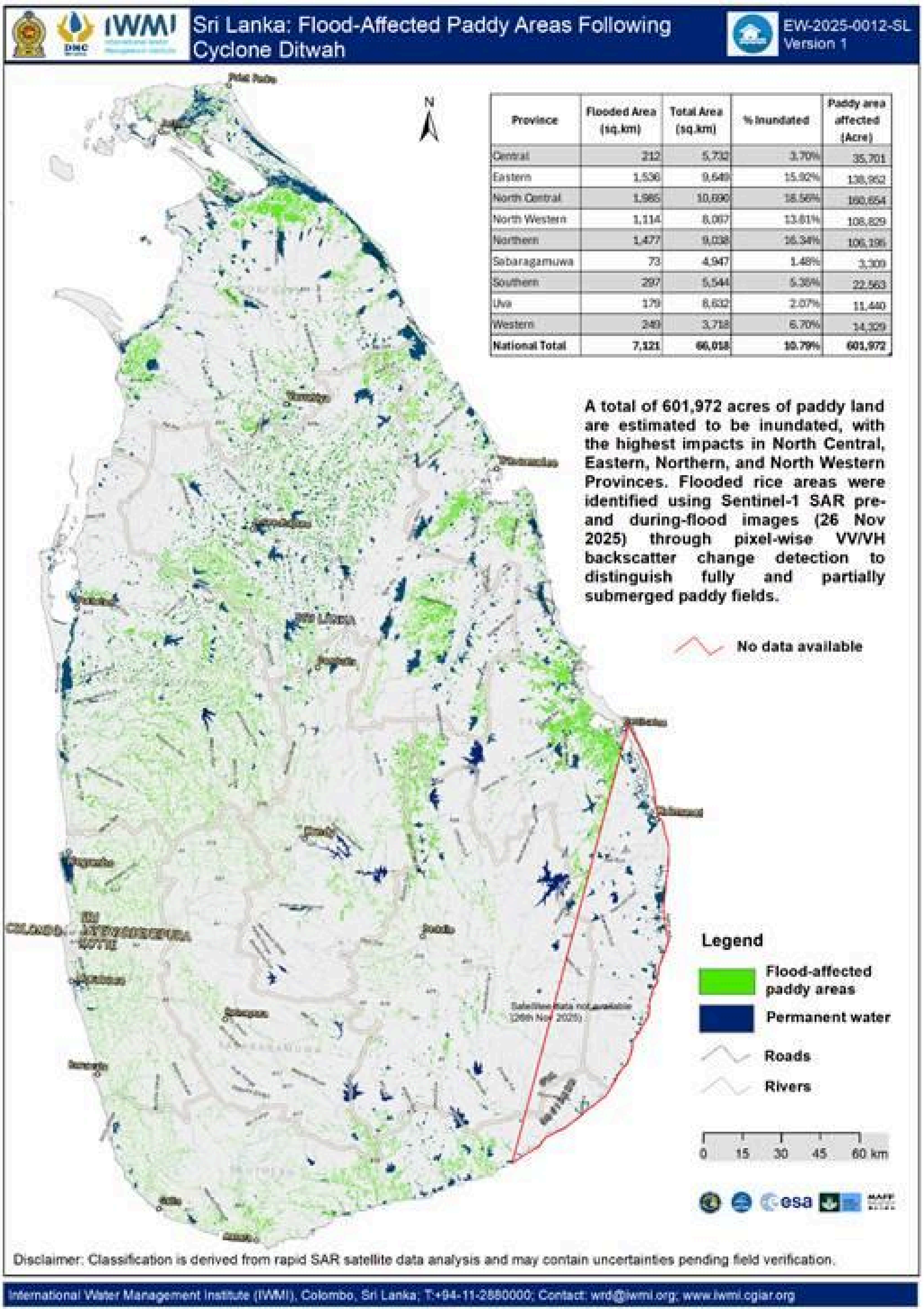

Figure A2: Flooded paddy lands after Cyclone Ditwah (IWMI SAR analysis). An estimated 601,972 acres of rice paddy were inundated nationwide. The map shows that North Central, Eastern, Northern and North Western provinces suffered the greatest paddy losses. Flooded rice fields were identified via Sentinel-1 SAR (VV/VH) change detection comparing pre- and during-flood imagery (26 Nov).

Table A2: Provincial Summary of Flood-Affected Paddy Area After Cyclonic Storm Ditwah

Province	Flooded Area (sq.km)	Paddy Area Affected (Acres)
North Central	1,985	160,654
Eastern	1,536	138,952
North Western	1,114	108,829
Northern	1,477	106,195
Central	212	35,701
Southern	297	22,563
Western	249	14,329
Uva	179	11,440
Sabaragamuwa	73	3,309
National Total	**7,121**	**601,972**

Hydrological Extremes

GloFAS-based streamflow data (via IWMI's AWARE platform) show that river flows in early Dec 2025 reached record levels across the island. In the Kelani River basin (Colombo area), gauges indicated critical flood stages: for example (See below flood forecast figures), at Kaduwela (Nagalagam Street station) the river surged to ~7.05 ft (~2.15 m) on the morning of 30 Nov, crossing the major flood threshold. Upstream at Hanwella, the Kelani peaked at ~10.88 m around 6:00 am (30 Nov), again at major flood level. These extreme water levels correspond to very high discharges. Indeed, reports confirm that the Kelani "burst its banks" on Friday 29 Nov, inundating parts of Colombo and adjoining suburbs. In the Maha Oya (north-western catchment), the flood was similarly unprecedented: authorities warned of "a potentially high-risk flood situation of a severity not experienced in recent times" in the Maha Oya valley. (Maha Oya catchment flows would have far exceeded normal peaks, given that warning.) The Mahaweli River at Manampitiya (Polonnaruwa) also saw very high flows: national forecasts extended flood warnings in the Mahaweli basin through Dec 3 due to continued rainfall. In summary, all four key monitoring points (Kaduwela & Hanwella on the Kelani, Maha Oya at Pannala, and Mahaweli at Manampitiya) recorded anomalously high discharges. While exact return-period analyses require long-term gauge data, these peaks clearly exceeded typical design flows. In fact, officials noted that the 2025 flood levels were expected to be even worse than those in the 2016 floods. Such evidence indicates extreme hydrological severity – likely rare (decadal or greater) events – consistent with the massive inundation seen.

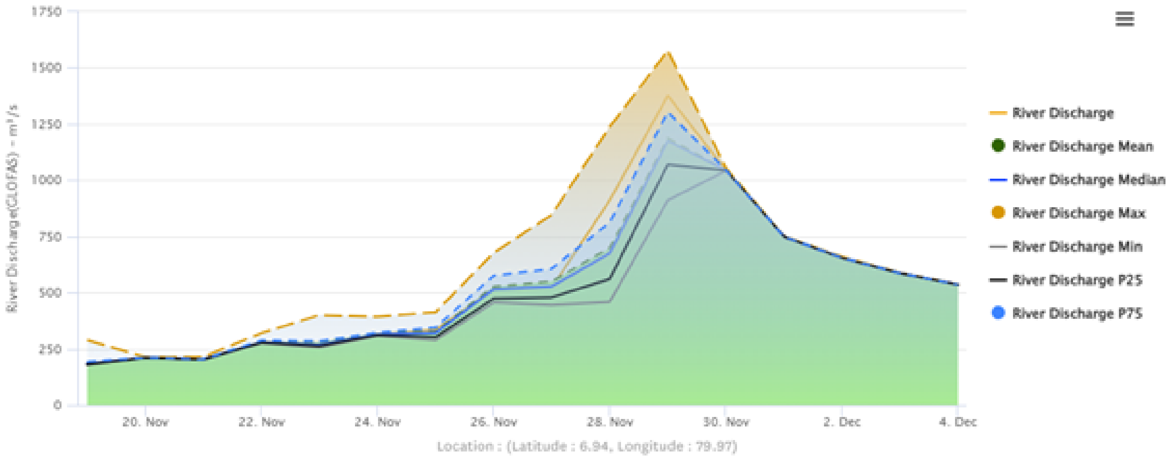

Location: Kaduwela, Kelani River basin

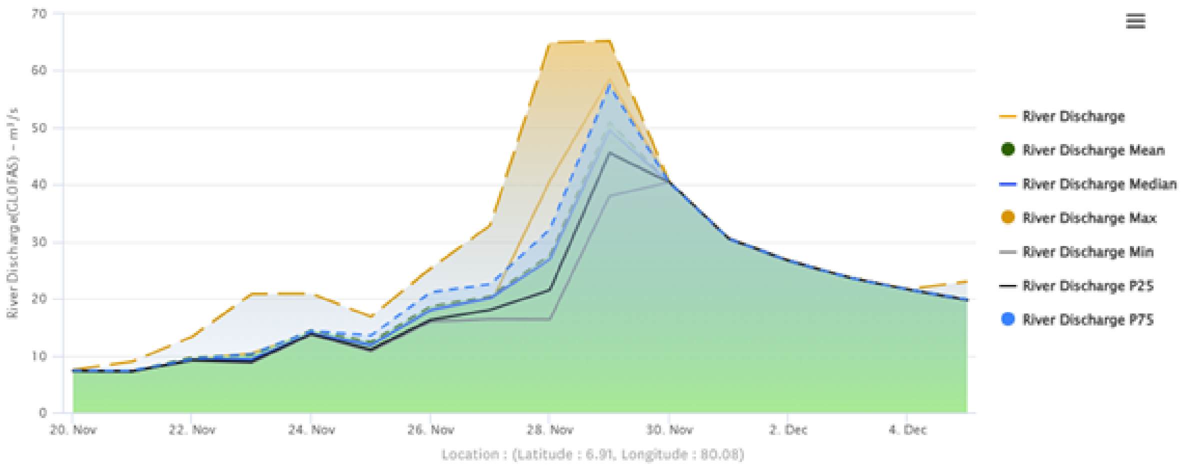

Location: Hanwell, Kelani River basin

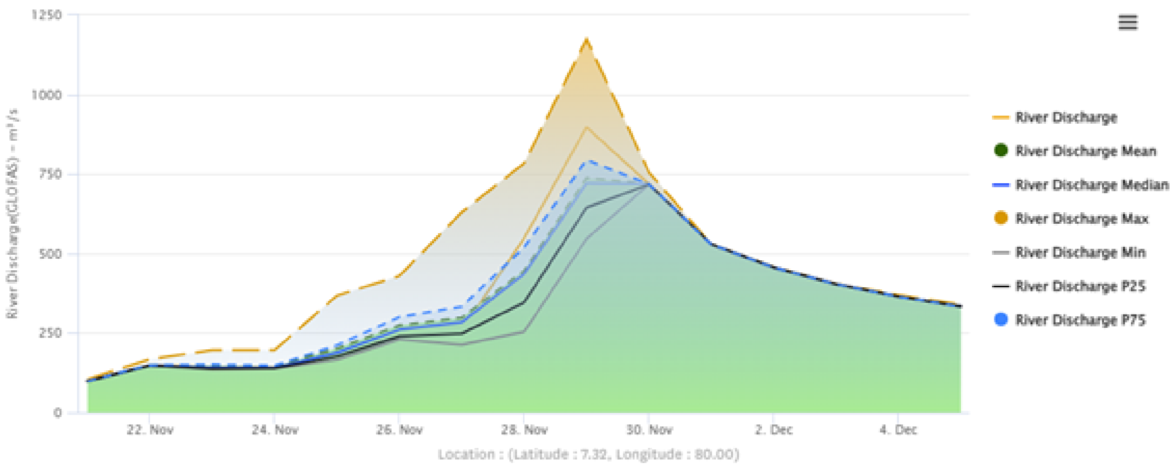

Location: Maha Oya, Pannala, Kurunegala district

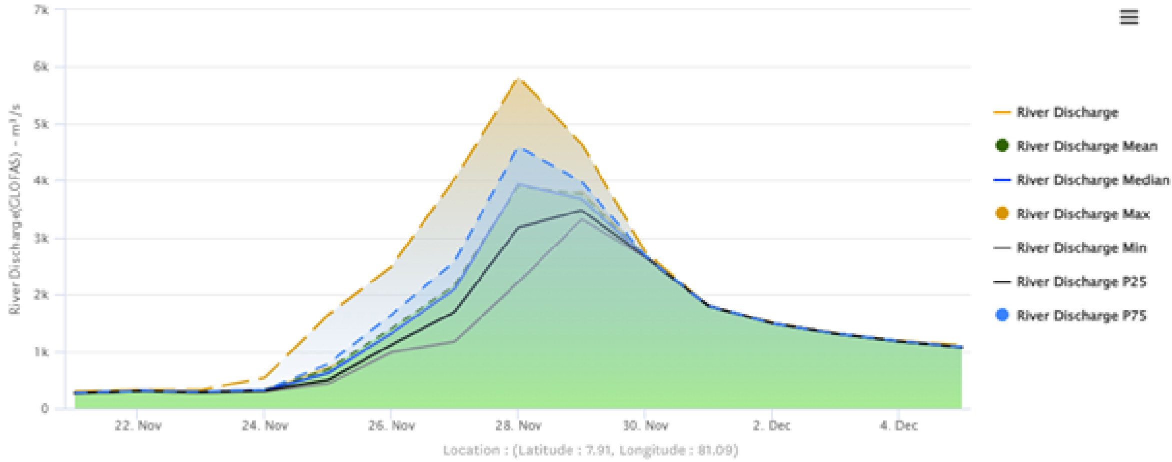

Location: Mahaweli river, Manampitiya Bridge, Polonnaruwa district